Electrochemical Characterization of Anode-respiring *Geobacter sulfurreducens* and *Geoalkalibacter subterraneus*

by

Oluyomi Ajulo

A Thesis Presented in Partial Fulfillment
of the Requirements for the Degree
Master of Science

Approved August 2013 by the
Graduate Supervisory Committee:

Cesar Torres, Chair
David Nielsen
Rosa Krajmalnik-Brown
Sudeep Popat

ARIZONA STATE UNIVERSITY

August 2013

ABSTRACT

To further the efforts producing energy from more renewable sources, microbial electrochemical cells (MXCs) can utilize anode respiring bacteria (ARB) to couple the oxidation of an organic substrate to the delivery of electrons to the anode. Although ARB such as *Geobacter* and *Shewanella* have been well-studied in terms of their microbiology and electrochemistry, much is still unknown about the mechanism of electron transfer to the anode. To this end, this thesis seeks to elucidate the complexities of electron transfer existing in *Geobacter sulfurreducens* biofilms by employing Electrochemical Impedance Spectroscopy (EIS) as the tool of choice. Experiments measuring EIS resistances as a function of growth were used to uncover the potential gradients that emerge in biofilms as they grow and become thicker. While a better understanding of this model ARB is sought, electrochemical characterization of a halophile, *Geoalkalibacter subterraneus* (*Glk. subterraneus*), revealed that this organism can function as an ARB and produce seemingly high current densities while consuming different organic substrates, including acetate, butyrate, and glycerol. The importance of identifying and studying novel ARB for broader MXC applications was stressed in this thesis as a potential avenue for tackling some of human energy problems.

ACKNOWLEDGMENTS

First and foremost, I thank God for without him, nothing is possible. I am grateful for the guidance I have received from Dr. Cesar Torres and for the opportunity he granted me to be a part of the Swette Center for Environmental Biotechnology (SCEB) community. I also owe a great deal of gratitude to Dr. Jon Badalamenti and Dr. Sudeep Popat for their tireless efforts in training me and their willingness to answer my questions regarding my projects; thereby contributing immensely to my work. I would be remiss if I do not thank my committee members, Dr. Cesar Torres, Dr. Sudeep Popat, Dr. Rosa Krajmalnik-Brown and Dr. David Nielsen, for taking time out of their busy schedules to attend to my concerns and for their contributions to this work. I am thankful for my colleagues in the SCEB lab and Diane Hagner, our lab manager, for providing support, stimulating conversations and comic relief when needed. Lastly, I thank my family for their relentless support. May God bless you all!

TABLE OF CONTENTS

Page

LIST OF TABLES vi

LIST OF FIGURES vii

CHAPTER

1 INTRODUCTION 1

2 BACKGROUND 11

3 MATERIALS AND METHODS 29

4 ELECTROCHEMICAL IMPEDANCE SPECTROSCOPY – RESULTS AND DISCUSSION 37

5 *GEOALKALIBACTER SUBTERRANEUS* CHARACTERIZATION RESULTS AND DISCUSSION 53

6 RECOMMENDATIONS FOR FUTURE WORK 66

REFERENCES 69

APPENDIX

A CHARACTERISTIC DIFFERENCES IN *GLK. FERRIHYDRITICUS* AND *GLK. SUBTERRANEUS* 74

B ELECTROCHEMICAL IMPEDANCE SPECTROSCOPY RESULTS OF REPLICATE EXPERIMENTS 76

LIST OF TABLES

Table Page

1. 4.1: *Geobacter* Biofilm Thickness and Current Density Relationship 49

2. 5.1: *Glk. subterraneus* Electron Donors Parametric Comparison 64

LIST OF FIGURES

Figure		Page
1.	1.1: Electron Tower	3
2.	1.2: MXC Schematic	4
3.	1.3: Reactor Types	5
4.	1.4: EET Mechanisms	7
5.	2.1: Potentiostat Schematic	13
6.	2.2: Typical Chronoamperometry	14
7.	2.3: CV Schematic	16
8.	2.4: CVs and Scan Rates	17
9.	2.5: CV and Energy Lost	18
10.	2.6: Randles Circuit Schematic	22
11.	2.7: Typical Impedance Responses	23
12.	4.1: Nernst Monod and U-Shapes	38
13.	4.2: *Glk. Subterraneus* Triple U	40
14.	4.3: *Geobacter* U-Shape	42
15.	4.4: *Geobacter* Growth Curves	44
16.	4.5: *Gebacter* CVs	44
17.	4.6: Nyquist Plot (labeled resistances)	46
18.	4.7: *Geobacter* Ohmic Resistance	47
19.	4.8: *Geobacter* Charge Resistance	48
20.	4.9: *Geobacter* Capacitance	51

Figure Page

21. 5.1: *Glk. subterraneus* Chronoamperometry (Acetate) 56

22. 5.2: *Glk. subterraneus* Chronoamperometry (Butyrate) 59

23. 5.3: *Glk. subterraneus* Chronoamperometry (Glycerol) 61

24. 5.4: *Glk. subterraneus* CVs (Acetate)..... 62

25. 5.5: *Glk. subterraneus* CVs (Butyrate)..... 62

26. 5.6 *Glk. subterraneus* CVs (Glycerol)..... 64

CHAPTER 1

INTRODUCTION

Over the centuries, humans have developed an insatiable appetite for energy in order to make daily life less rigorous. From the advent of coal burning and the industrial age, our cravings for energy have consistently increased. In fact, some of our energy resources are being consumed rather quickly and also being produced at a remarkable rate (Welch et al., 2005) as the world's population continues to increase. While critics, scientists and even the general public argue constantly about having enough to sustain daily life for centuries or even decades to come, we, as a people, have recognized that we have a challenge/mandate to search for alternatives to subsidize and possibly replace our fossil fuels.

To meet this challenge of replacing fossil fuels with more renewable energy sources, we can utilize microorganisms since they have the ability to generate energy from renewable sources of biomass that do not disrupt the human food-supply systems (Chynoweth et al., 2001; Logan, 2004). There exist communities of organisms that convert biomass to useful energy forms such as hydrogen, methane and electricity (Rittmann, 2008) and since we generate agriculture waste and food processing industries wastes, there is an abundant amount of biomass substrate for these organisms (Rittmann et al., 2008). The ability of microorganisms to generate energy from the oxidation of organic compounds can be applied to the degradation of the waste we generate from human activities. While some of these bacteria possess the ability to use organic wastes compounds as carbon sources, others are able to utilize them as electron donor sources or electron acceptors. Studies have shown that the degradation of these compounds happen quicker if oxygen is present, but in high-strength wastes and subsurface environments, the probability that oxygen will be available is

very slim, therefore, the degradation of these compounds have to rely on organisms that do not need oxygen to function (Lovley, 2000; Siegert et al., 2010).

Anaerobic organisms can use a variety of compounds as their electron acceptors such as nitrates, sulfates, iron, manganese and even uranium. The choice of the electron acceptor depends on the electron donor available in the environment and on the energetics of the donor/acceptor couple. This is the reason why hydrogen and oxygen are nature's choice for electron donor and acceptor couple; an organism gains the most energy with this couple (Figure 1.1) (Madigan et al., 2009). There are anaerobic organisms that couple the reduction of metals most common in nature to the oxidation of simple organics. These are termed dissimilatory metal reducing bacteria and a few of these have been extensively studied. *Shewanella oneidensis*, a freshwater organism, is known to couple the oxidation of organics to the reduction of manganese, Mn (II). In fact, it has become the star of this process (Kostka et al., 1995; Lin et al., 2012). Iron is an electron acceptor that is more readily available than manganese (Figure 1.1), hence, there have been numerous studies focusing on iron-reducers and their ability to oxidize a diverse set of donors. A known dissimilatory iron reducing organism of this sort, *Geobacter sulfurreducens*, was first isolated in 1994 from surface sediments of a hydrocarbon-contaminated ditch in Norman, Okla (Caccavo et al.,1994). It is a gram-negative bacterium, nonfermentative, nonmotile and also a freshwater organism. This organism has since been known as *G. sulfurreducens* PCA and it was found to be able to not only reduce solid acceptors such as elemental sulfur and Fe (III) oxide, but also a few other soluble iron forms, such as iron citrate and iron pyrophosphate, when coupled to the oxidation of acetate or hydrogen. This ability to respire to a solid acceptor outside of the cell has made this genus a prime target for electrochemists and microbiologists interested in

bioremediation. In these circles, these bacteria are known as Anode Respiring Bacteria (ARB) because they can be used in fuel cells and electrochemical cells to harness their energy.

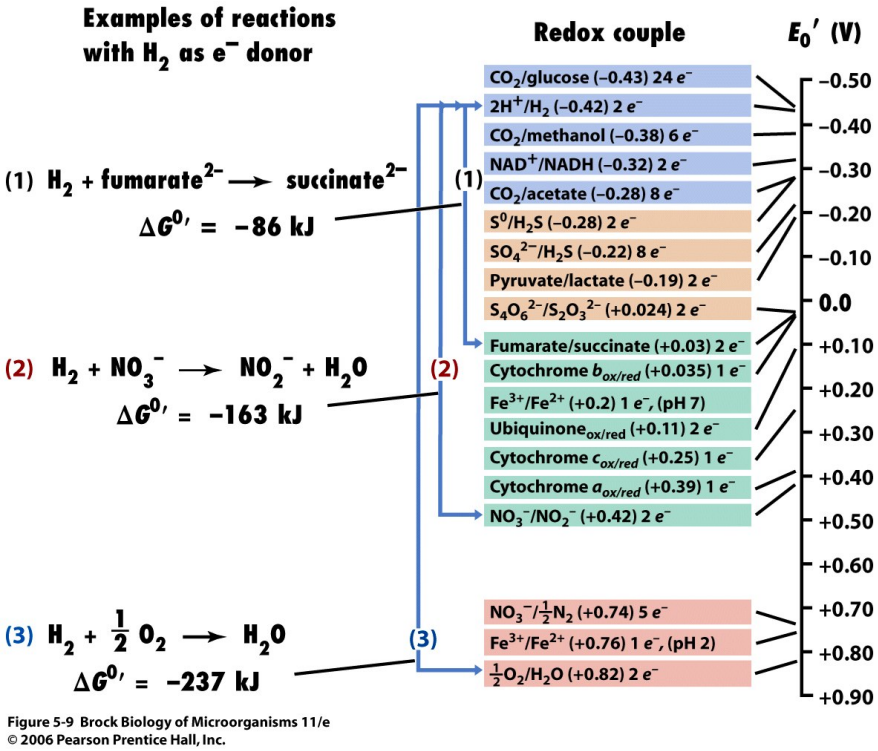

Figure 1.1. The electron tower showing various redox couples and their reduction potential with the most reduced, hydrogen, at the top and the most oxidized, oxygen at the bottom of the tower. Source: Madigan et al., 2009

As a general definition then, ARB are anaerobic bacteria that possess the ability to couple the oxidation of organic compounds such as acetate or hydrogen (electron donor) to electron transfer to an anode that is positioned outside of the cell. ARB are used in microbial electrochemical cells (MXCs) to transform energy from that which is stored in the organic compounds to electrical energy through cells growing on the electrodes (Figure 1.2). With the use of a potentiostat, the anode is usually poised at a specific redox potential that will

allow for current dispersed to be measured as the bacteria transfer electrons onto the anode. Therefore, the anode is their terminal electron acceptor.

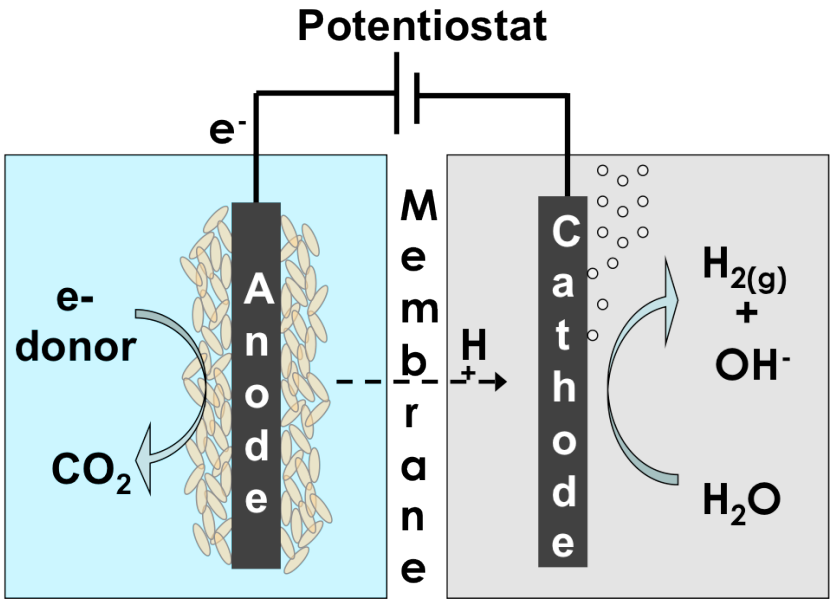

Figure 1.2. Schematic of an MXC showing the complete oxidation of an electron donor to carbon dioxide while the electrons released are transferred to the cathode to split water into hydrogen gas and hydroxide ions. The potentiostat is used to maintain the anode at a potential conducive for the oxidation of the electron donor. The two chambers are separated with a membrane to provide a medium for ion transport.

Adapted from Torres et al., 2010.

MXCs take on very different designs specific to the objective of the study as will be outlined in the next few chapters and displayed in Figure 1.3. There are H-type reactors that allow for the isolated control of the electrode of interest, which is the anode in most cases. These are mostly used to study kinetic and thermodynamic parameters. There are other designs that allow for more in-depth fundamental electrochemical studies. These types are usually single chamber ones where both electrodes exist in the same electrolyte. Both of the reactors discussed here are shown in Figure 1.3 below.

MXC applications require having fundamental knowledge of the mechanisms involved in electrical current production by ARB. Thus, researchers in the field are constantly trying to improve our understanding of ARB, by characterizing their behavior in MXCs. MXCs and the ARB that grow in them have a long way to go to make their mark in the industrial setting because of scale-up constraints and the ability to minimize potential losses in all chambers of the reactors. Overall, an efficient MXC need be one that is able to minimize resistances that can originate from the anode, cathode or the electrolyte. Later in this document, I discuss our work on the identification of resistances as it relates to the ARB anode (Chapter 4).

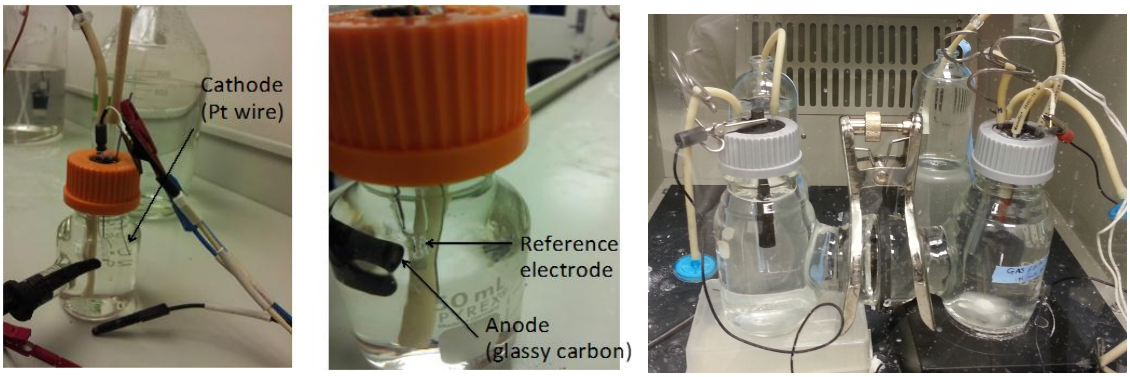

Figure 1.3. On the left, a single chamber small (50 mL, 3.14 mm^2 anode size) reactor used for fundamental characterization of ARB. A zoomed in version of this reactor is shown in the middle picture. On the right, an H-type MEC (350 mL, 5.27 cm^2 anode size) is shown with the anode chamber (right chamber) and the cathode chamber (left) separated by an anion exchange membrane.

There have been many spirited debates in the MFC community since the late 90s about the mechanism of electron transfer from the biofilm formed by these bacteria to the electrode (Lovley,1991). Some ARB do not form a biofilm, but the ones that do must have a conductive ability responsible for their current generation. To this end, there are in fact three

different mechanisms of extracellular electron transfer (EET) proposed and mostly accepted by the scientific community namely, direct electron transfer by a monolayer of cells, shuttling and long range electron transfer. These mechanisms can fit under two umbrellas, direct electron transfer (DET) and mediated electron transfer (MET) (Barton, 2010; Ferapontova et al., 2005).

In DET, the microbes are said to have enzymes or other redox active structures overlapping to increase the probability of electron transfer to the electrode (Dominguez-Benetton et al., 2012; Ferapontova et al., 2005). Under this broad umbrella mechanism is that of long-range electron transfer by way of either nanowire like proteins, pili, or redox active cytochromes that allow electrons to hop to the electrode (Logan et al., 2009). MET, on the other hand, refers to the microorganisms being able to produce soluble compounds acting as shuttles of electrons between the biofilm and the solid iron outside of the cell. As part of MET mechanism, some organisms produce chelators instead of electron shuttles for the sole purpose of solubilizing the solid iron into the form that the organism can now bring into its cell (Dominguez-Benetton et al., 2012; Marsili et al., 2008). A schematic of these mechanisms is shown below with DET and MET mechanisms clearly labeled (Fig. 1.4.)

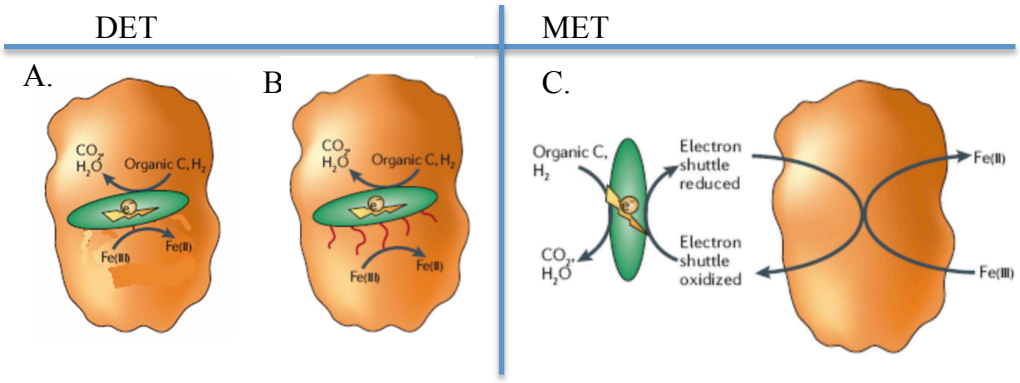

Figure 1.4. The three mechanisms proposed for extracellular electron transfer are outlined with (A) Direct contact in this case with the solid iron and (B) Microbe using nanowire like structures to make contact with the solid iron; representing the DET mechanisms. (C) Microbe producing electron shuttles represent MET. Source: Weber et al., 2006

The *Shewanella* genus has been studied enough to uncover most of the EET mechanisms these bacteria use. *Shewanella* can use two out of the three mechanisms listed above to do EET. *S. oneidensis* MR-1 has been shown to primarily use shuttles (Logan, 2009; Marsili et al., 2008), *S. putrefaciens* was thought to primarily use outer membrane cytochromes to make contact (Kim et al.,1999; Lovley,1991; Myers and Myers,1992), and recently *S. liohica* has been explored with regards to its mechanism of electron transfer (Jain et al., 2013). In this study, it was shown that the mechanism could change for the same organism depending on the material of the electrode they respire. With the aid of few electrochemical methods, mainly cyclic voltammetry (CVs) and differential pulse voltammetry (DPV), the authors discovered the dominant mechanism to be DET when the electrode used was an indium tin oxide (ITO) electrode, while on graphite electrodes, a mixture of DET and MET was observed. The mixture of mechanisms here actually leans towards MET (Jain et al., 2013).

They attributed this difference to the roughness of the graphite electrode lending itself to the adhesion of compounds like flavins and quinones.

Unlike *Shewanella*, the *Geobacter* genus has caused more controversy. *Geobacter* only uses DET, but researchers have thoroughly discussed the details of how DET is occurring. Some believe strongly that *Geobacter* indeed secrete conductive nanowires, allowing them to form a electrochemically active biofilms able to generate electricity as well as produce high current densities (Malvankar and Lovley, 2012; Reguera et al., 2005). On the other hand, there is another school of thought that seems to align with redox proteins participating in electron hopping (Liu and Bond, 2012). From a 2010 study determining kinetic processes of ARB depending on their EET mechanisms, it was clear that for an ARB to use direct contact for its EET mechanism, it cannot form thick biofilms and neither can it produce high current simply because it cannot accumulate enough active biomass (Torres et al., 2010). Conversely, for ARB that produce high current and has minimum potential losses, as *Geobacter* do, solid conduction is most likely to be the EET mechanism. In Bond et al. 2012, many experimental evidence for *Geobacter* actively respiring were considered and they determined that the change of local pH values in the biofilm has an effect on respiration as it related to the fraction of oxidized cytochromes to accept electrons from cells. This shows the importance of cytochromes in the EET mechanism of *Geobacter*.

While much is known about *Geobacter spp.*, there is still many unknowns about the outer membrane cytochromes, especially which ones are directly responsible for the electron transfer of these biofilms (Torres et al., 2010). Thus, a specific aim of my Thesis was to further characterize *Geobacter sulfurreducens* using electrochemical impedance spectroscopy (EIS). EIS is a novel electrochemical method that separates specific electron-transfer

resistances through an analysis of sinusoidal AC currents. My goal was to elucidate key electron-transfer processes through EIS, some of which could be associated with EET (Chapter 4).

Regardless of the mechanism of electron transfer, ARB have seemingly vast applications through MXCs. Unfortunately, only *Geobacter* strains have been shown to produce high current densities in MXCs, thus substantiating the feasibility of such applications. The disadvantage with *Geobacter* is its limited set of electron donors; consequently, there is an important need to find more ARB to increase the functional diversity of the microbial communities developed in MXC anodes. While *Geobacter sulfurreducens* is a freshwater microorganism that grows at neutral pH, other potential electron donors in other environments, specifically saltwater, may not necessarily fit the profile of *Geobacter*. Therefore, the MXC community should not only focus on finding different ARB, but on finding those that can grow under different environmental conditions and utilize a wide variety of electron donors. In Chapter 5, I will discuss my work characterizing one such novel ARB, *Geoalkalibacter*, which is a halophilic ARB capable of consuming a wide variety of electron donors.

In the next few chapters, I will outline and discuss my Thesis work aiming at characterizing electron-transport processes in *Geobacter* and characterizing a novel halophilic ARB, *Geoalkalibacter subterraneus*. Chapter 2 is a background of ARB currently studied, the anode respiration capability of which has been discovered in our lab, and the various electrochemical methods we use to characterize them. Chapter 3 outlines the experimental methods and materials used in the studies presented. Chapter 4 presents the results and discussion of the *G. sulfurreducens* characterization using EIS. Chapter 5 details my efforts in

characterizing a new bacteria genus, *Geoalkalibacter spp.*, as an ARB. Finally, I discuss some future directions for both organisms central to this work in Chapter 6.

CHAPTER 2

BACKGROUND

There are ARB that can generate appreciable current densities like *Shewanella Oneidensis* and *Desulfuromonas spp*. However, it is *Geobacter sulfurreducens* that is able to produce nearly 10 times more current densities than any other ARB characterized so far (Torres et al., 2010). For this reason, our research group sought to find other efficient ARB and this quest started with mixed microbial communities. We investigated 13 different samples from Romania, India, Japan, United States and Puerto Rico representative of different environmental conditions (Miceli et al., 2012). Some of these samples came from saltwater areas while some came from freshwater regions. Using the enrichment technique previously described in an earlier work, highly efficient ARB were enriched as major components of the different mixed cultures. About half of these cultures were able to produce high current densities (>1.5 A/m^2). This lends to the idea that ARBs can be isolated from these cultures that could potentially rival current densities produced by *Geobacter* and have variety of applications especially in different ecosystems. It is well known that although *Geobacter* is somehow ubiquitous, it is not optimized to function in high salinity regions and non-neutral pH conditions. Since the applications for ARB capabilities are constantly expanding, it is imperative that the ARB library expands to involve these otherwise extreme conditions for the current ARB. From the seven cultures that produced high current densities, there were two in particular from saltwater environments, namely Carolina Mangrove and Salt Flat, both from Puerto Rico. The respective current densities from these two cultures were approximately 11 A/m^2 and 8 A/m^2 respectively. These were the highest current densities from our samples, and among the highest current densities reported in literature (Katuri et

al., 2012; Parameswaran et al., 2010). Therefore, it is expected that we would want to investigate these cultures further.

From the pyrosequencing data presented in this work(Miceli et al., 2012), it was determined from the sequences that the microorganism dominant in these culture enrichments were from the family *Geobacteraceae*, but in the genus *Geoalkalibacter*. Because these samples were obtained from saline regions, they were enriched with 2% NaCl saline media. From what is known about the organisms belonging to this genus, pH is an important factor since they are alkalitolerant/alkaliphilic. Thus, it was exciting to find other organisms that could respire the anode with the next steps being isolation and further characterization. Specific isolated species in this genus will be discussed later to thoroughly explain their capabilities (Chapter 5).

There are a few electrochemical methods of characterization that have proven quite useful; namely, chronoamperometry, cyclic voltammogram and electrochemical impedance spectroscopy. These methods tend to provide information regarding possible electron-transfer mechanisms, midpoint potentials and other processes inherent to that particular microbial system. In the microbial ecological analysis reviewed above, two of the methods were used hand in hand to obtain the effective maximum current densities (j_{max}) of these systems: chronoamperometry and cyclic voltammetry.

- Chronoamperometry

In any electrochemical circuit, there are only two parameters that can be varied as a function of time: voltage and current. Chronoamperometry is the measurement of current as a function of time while the potential is held constant. In the work presented, the anode potential was controlled with a potentiostat (VMP3, Biologic, USA) at -0.30 vs. Ag/AgCl,

but was interrupted to perform other electrochemical measurements. The potentiostat is an electronic instrument used to control an electrochemical cell, studying the processes taking place on the working electrode (anode in this case) without interference from the counter electrode. It measures and controls the voltage difference between a working electrode and a reference electrode.

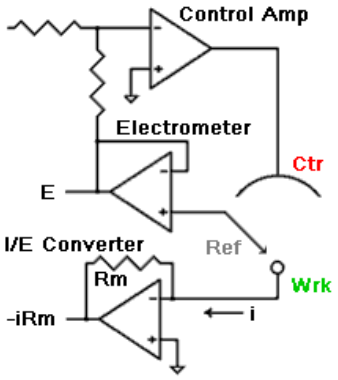

Figure 2.1. Simplified schematic of the circuitry of a potentiostat. Source: http://www.consultrsr.com/resources/pstats/design.htm

A potentiostat has three important parts; a control Amplifier, an electrometer and a current/potential (I/E) converter. The control amplifier supplies power to control the potential between the working and the reference electrode while the electrometer measures this potential difference. The I/E converter is the part that now measures the current between the working and counter electrodes. This process of measuring and adjusting potentials is a control loop that is repeated throughout the duration of the experiment to keep the potential of the working electrode constant. This control loop has a time scale of microseconds to milliseconds, whereas our MXC current density is measured every two minutes (Figure 2.2). In MXCs, the choice of potential to set the anode is directly related to

the potential of the organic substrate that is used. For instance, the substrate Miceli et al., (2012) used was acetate with a standard reduction potential of approximately -0.550 vs. Ag/AgCl; therefore, it is sensible that the anode was poised at a potential higher than that of acetate. Maintaining a constant potential while current is recorded produces a graphical representation much like Figure 2.2. This data gives information regarding the performance of the MXC with the time progression.

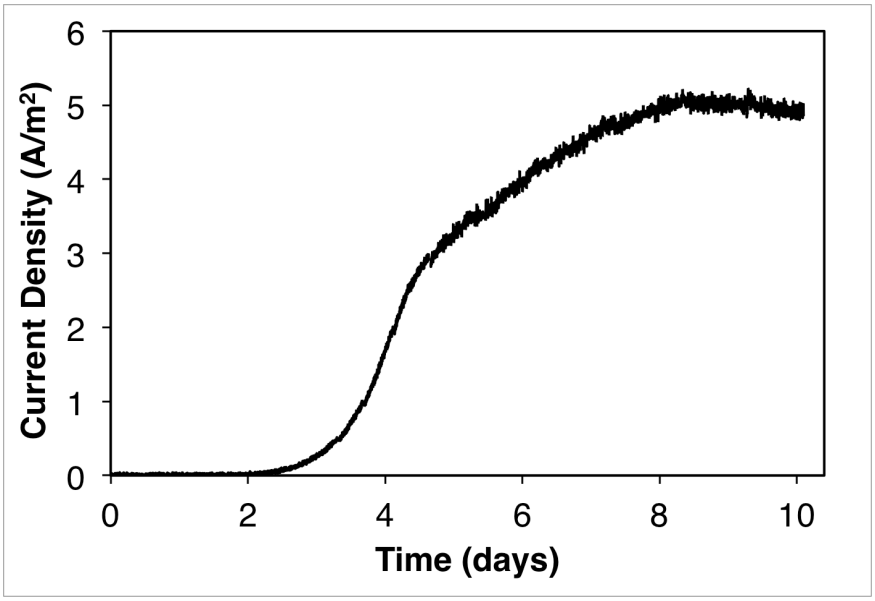

Figure 2.2. Chronoamperometry showing current evolution of a *Geobacter sulfurreducens* biofilm grown on a gold electrode at -0.02V using 10mM acetate as electron donor and media buffered with 30mM bicarbonate.

In this case, the maximum current density is approximately 5 A/m^2. Aside from this information, we can glean from a plot like this is that the ARB growth is exponential, as the current increases exponentially. Further analysis can be done to obtain other useful information about the microorganism such as its doubling rate. The integration of the

current production above provides the total electron equivalents respired by the ARB, from which calculations of Coulombic efficiency and recovery can be obtained. However, information concerning the internal workings of the system cannot be extrapolated from a chronoamperometry plot. To obtain more information regarding kinetics and transport, more sophisticated methods must be used. In the next few sections, I will discuss two such methods: cyclic voltammetry (CV) and electrochemical impedance spectroscopy (EIS)

- Cyclic Voltammetry (CV)

CV is a method whereby the potential applied between the working electrode and the reference electrode is varied linearly with time at a predetermined rate. This ramping is known as the scan rate applied (V/s). As the potential is applied, the current is measured between the working electrode and the counter electrode. In normal practice, the potential is swept back and forth between two potential limits and the current measurement is recorded versus the potential (Figure 2.3). In times past, this method has been used to characterize the catalytic activity of different electrochemical catalysts (Lau et al., 2011). In theory, as the waveform is generated, the forward scan should produce a current peak of the analytes that can be oxidized in the system in the potential range that has been set. As the forward scan is generated, the current increases as the potential reaches the oxidation potential of the analyte in solution. However, once this particular analyte consumed at the electrode surface, the current will decrease, creating an oxidation peak. A steady oxidation current (positive) will then be observed that is the result of the rate of transport of the analyte to the electrode surface. On the reverse scan, this analyte will now be reduced; therefore, the opposite happens and another current peak shows up closer to the lower limit of potential range.

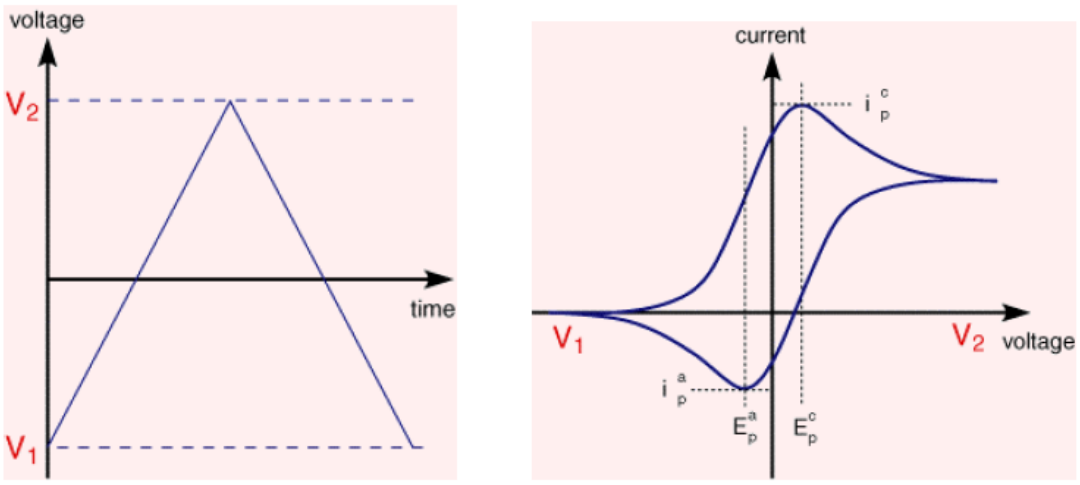

Figure 2.3. On the left is a graphical representation of the cycling of potentials as a cyclic voltammogram (CV) is obtained. The potential increases and decreases with time. On the right is an example of a classical CV with the forward and reverse scans. Source: O'hayre et al., 2009

If the redox reaction occurring at the electrode is completely reversible, the peak currents shown above will be spaced by 58 mV for a one-electron reaction. A system is reversible when the electrochemical redox reaction is fast enough to maintain the concentration of oxidized and reduced species at equilibrium with each other at the electrode surface (Mabbott 1983). According to the Randles-Sevcik equation, the peak current is directly related to the square root of the scan rate (Mabbott 1983).

$$i_p = (2.69 \times 10^5)\, n^{3/2} A\, D_0^{1/2} \nu^{1/2} C_0^* \qquad (2.1)$$

Here, i_p is peak current in (Amp), n is the number of electrons involved in the redox reaction, A is the electrode area in (cm^2), D_0 is the diffusion coefficient, ν is the scan rate (V/s) and C_0* is the bulk concentration (mol/L). This equation relates the peak current to the diffusion of substrate to the anode surface. Thus, a relationship between transport (i.e. diffusion coefficient) and the CV peak current can be performed. As illustrated in Figure 2.4, as the scan rate is increased, the peak current also increases, but not the potential. The different peak currents obtained as a function of the square root of the scan rate gives a line with a slope proportional to the diffusion coefficient.

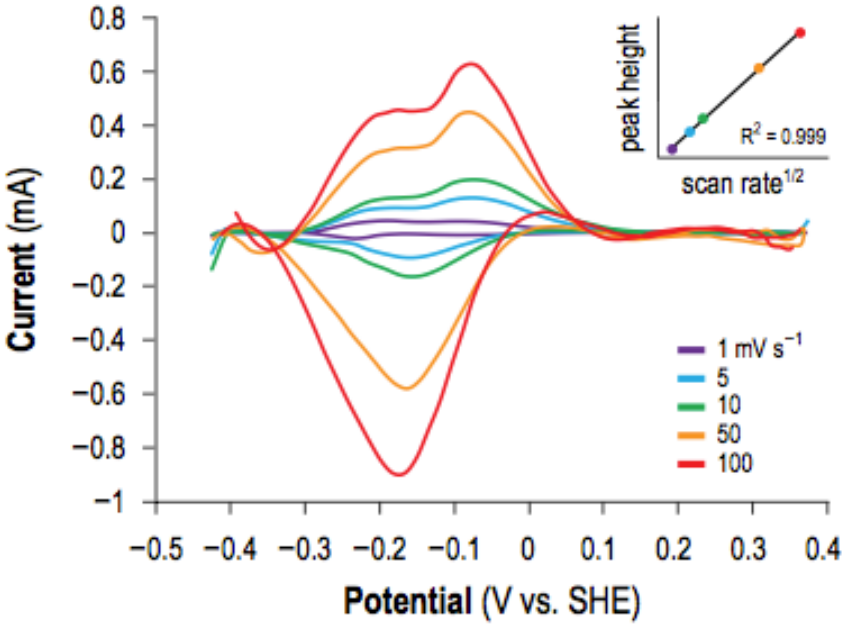

Figure 2.4. Here, a derivative CV of *Glk. ferrihydriticus* grown using 10mM Acetate is shown with peak current (minima and maxima) increasing as the scan rate is increases from 1 mV/s to 100 mV/s. The linear relationship between the peak current (peak height) and the square root of the scan rate is shown in the right corner. Source: Badalamenti et al., 2013

Cyclic voltammetry can be performed at both steady state and non-steady state conditions. Under non-steady state conditions, which are where most of the measurements are obtained, we get variety of information from the CVs, such as those obtained through the Randles-Sevcik Equation (Nicholson and Shain, 1964). In MXCs, we use the CV to determine different kinetic parameters of the biofilm growing on the anode and we also use it to observe any redox active molecules in the system that will invariably produce current peaks as the scan is generated. Under steady state conditions (at lower scan rates), we can obtain what is known as a j-V curve, providing information closely related to the conditions at which the MXC is being run. These plots are often sigmoidal (Figure 2.5), showing that there are potential losses in the system.

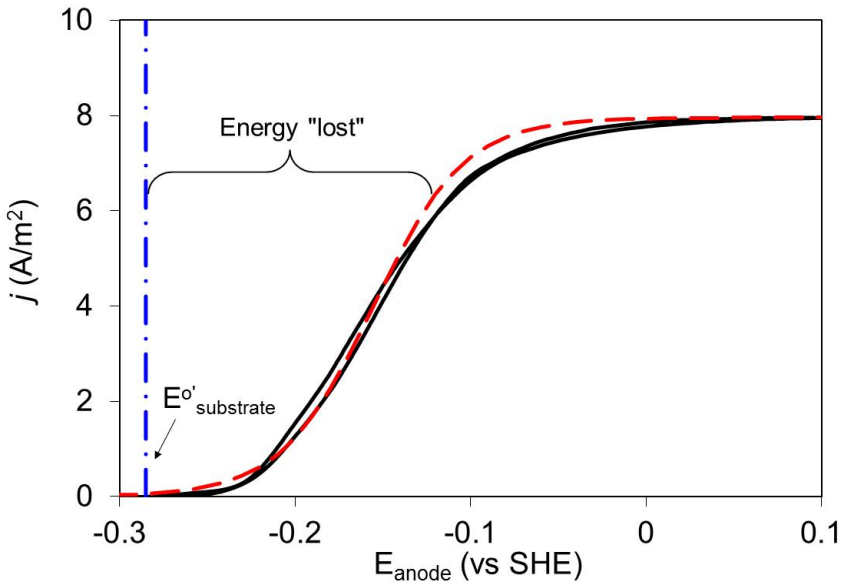

Figure 2.5. A mixed culture of ARB biofilm grown on acetate showing a classic CV and the energy lost to other processes not contributing to current generation. (Torres et al., 2010)

To model this sigmoidal shape, our lab developed a relationship relating the Nernst equation and Monod kinetics to describe microbial growth. This relationship is known as the Nernst-Monod model and it assumes that there is a redox process determining the energy that an ARB can recover from respiring on the anode using a simple organic substrate.

$$j = \frac{j_{\max}}{1 + \exp\left[\frac{-nF}{RT}(E - E_{KA})\right]} \tag{2.2}$$

Here, j is current produced, E is the anode potential, $j_{\max}$ is the maximum current, n is the number of electrons transferred, F is the faraday's constant, R is the gas constant, T is the temperature and the E_{KA} is the potential at which j is half $j_{\max}$ or also known as the midpoint potential.

From steady-state CVs, we can obtain midpoint potentials (E_{KA}) and j_{max} of the system. These can differ for the same ARB consuming different substrates. It is also possible to get more information about the mass transport in the system. Although, a CV is a powerful tool and provides an estimate of potential losses at the electrode, we cannot segregate between the processes that are causing these potential losses. This is the reason why another method, electrochemical impedance spectroscopy, is used, oftentimes in conjunction with a few of the ones already discussed above.

- Electrochemical Impedance Spectroscopy (EIS)

Electrochemical Impedance Spectroscopy (EIS) is used to understand the potential losses of a particular electrochemical system. It describes the behavior of an alternating voltage or

current as a function of frequency (Dominguez-Benetton et al., 2012). As previously mentioned, in a standard j-V curve, one is privy to the general performance of the fuel cell, but the energy lost in each reaction and electron-transfer step is not known. The EIS theory has been applied to many fields; however, in this discussion, we will use EIS to characterize the model ARB, *Geobacter sulfurreducens,* as it respires the anode from the oxidation of acetate. Below, I outline a few concepts needed to understand the usefulness of this tool.

Impedance

Similar to resistance, impedance is the ability of the system to resist current. The difference lies in the fact that impedance has time and frequency dependence. According to Ohm's Law, resistance, R, is defined in direct current (DC) circuit as $R = V/i$, the ratio of Voltage and current and only the resistors cause a resistance to electron flow. However, impedance, Z is defined to be the ratio of the same parameters but with a time dependence, $Z= V(t)/i(t)$. In EIS, impedance is measured by applying a small alternate potential to an electrochemical cell. An alternate current (AC) is the result of this potential application. Here, resistors, capacitors and inductors all affect the current response, shifting the phase angle, Φ, of the sinusoidal response (Equation 2.2) (Orazem and Tribollet, 2008; O'hayre et al., 2009). The small potential applied, normally in the range of 5-20 mV, ensures the measurements stay in the linear region of the j-V curve. Impedance has both imaginary and real components as explained in the following derivation considering the time and frequency dependencies:

$$V(t) = V_0 \cos(\omega t) \tag{2.3}$$

$$i(t) = i_0 \cos(\omega t - \Phi) \tag{2.4}$$

$$Z = \frac{Vo\cos(\omega t)}{io\cos(\omega t - \phi)} \tag{2.5}$$

$$Z = Zo\frac{\cos(\omega t)}{\cos(\omega t - \phi)} \tag{2.6}$$

$$Z = Zo\frac{e^{j\omega t}}{e^{j\omega t}/_{e^{j\phi}}} \tag{2.7}$$

$$Z = Zo\, e^{j\phi} = Zo(cos\phi + j\, sin\phi) \tag{2.8}$$

$$Z_{real} = Zo\cos\phi \tag{2.9}$$

$$Z_{imag} = j\, Zo\sin\phi \tag{2.10}$$

Through this derivation, Euler's formula $(e^{jx} = \cos x + j\sin x)$ is used to separate the real and imaginary components of *Z* (Eq. 2.8). In a typical CV like that shown in Figure 2.5, the energy lost can be attributed to different processes, including Ohmic conduction, activation overpotential, and energy needed in mass transport. Most fuel cell systems can be modeled by a combination of simple Randles circuits where there are 3 elements, an Ohmic resistance between working and the reference electrode in solution, charge transfer resistance and a double layer capacitance; both at the interface between the electrode and the surrounding solution. Each of these circuits has its own contribution to the total impedance in the system (Orazem and Tribollet, 2008).

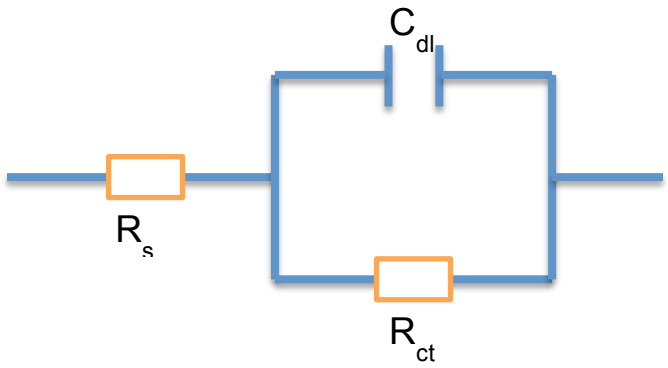

Figure 2.6. Simple schematic of Randles circuit, which includes a solution resistance, a double layer capacitor and a charge transfer. The double layer capacitance is in parallel with the charge transfer resistance.

The data obtained from EIS is typically a graphical representation of Z" (Z_{imag}) vs. Z' (Z_{real}) referred to as Nyquist plots. These plots do not give any frequency information. The impedance behavior of the system is summarized over many orders of frequency magnitudes. The only information regarding frequency one can glean from these plots is the general idea that from left to right, the frequency decreases. The information given by a Nyquist plot can be correlated to our equivalent circuit model. The first intersection of the semicircle with the Z_{real} axis gives the Ohmic impedance. The other charge-transfer resistances are more difficult to determine, as they are associated to a capacitance (Figure 2.6) that creates a frequency-dependent response in both real and imaginary Z components. This is exemplified by the semi-circle in Figure 2.7a, which is a typical response for a simple Randles circuit. More complex systems lead to a more complex Nyquist plot. Various fitting methods can be used to extrapolate the other resistances, but this method depends on the type of system being evaluated. This information can also be reported in a Bode plot as

shown in figure 2.7b. Unlike the Nyquist plot, the Bode plot has frequency and phase shift information.

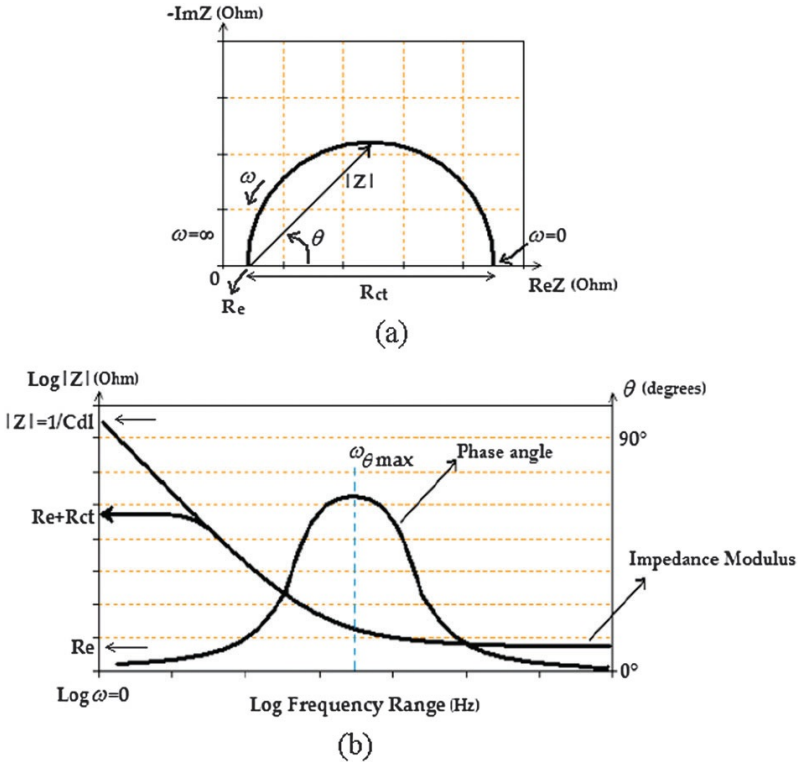

Figure 2.7. Typical impedance responses reported as (a) Nyquist plot: real impedance (Re Z) vs. negative of the imaginary impedance (-ImZ) and (b) Bode plot of the impedance: phase angle (y) and impedance modulus (|Z|) plots vs. frequency (ω) as an independent variable. Source: Dominguez-Benetton et al., 2012

In order to analyze the data generated from conducting EIS, there are a few assumptions of the system namely, linearity of the system, causality, and stability (Dominguez-Benetton et al., 2012; Macdonald, 2005; Orazem and Tribollet, 2008). To ensure that the system meets these requirements, a mathematical method, Kramer Kronig (KK) transform is used to verify its validity. The KK relations connect the real and

imaginary elements of any complex function. With these relations, the magnitude of the impedance can be calculated or parts of the function can be computed from whichever one is known, either real or imaginary. Since, impedance is a complex function, KK transforms prove useful in EIS data analysis. Specifically, they are used to check the validity of impedance spectra obtained over a wide range of frequencies(Macdonald, 2005; Orazem and Tribollet, 2008). If the magnitude of the impedance is known, the polarization resistance or the charge transfer resistance can be calculated directly from this data. This resistance can also be calculated indirectly from the imaginary portion of the impedance(Macdonald, 2005). Although this method is useful for obtaining pertinent information about electrochemical systems, a limitation may exist at the low frequency range, especially after 20Hz (Macdonald, 2005). It is important to keep in mind that the KK transforms do not provide or take into account any other physical properties of the system. If the above limitations are satisfied, then, the data generated should be correct. This is not to say that KK transforms is the only impedance validation technique; in fact, experimental, graphical and regression methods can be used to check whether the impedance data meets the KK assumptions (Dominguez-Benetton et al., 2012).

Till now, I have outlined how to report data from EIS measurements and also the importance of the information the measurements can potentially tell us about MXC systems. However, in our EIS studies (Chapter 4), we will expand upon the complexity of electron transfer in ARB through proteins. The process of transferring electron outside of the cell is one that is inundated with resistances from the proteins participating in the electron transfer, both intracellular and extracellular. These resistances lead to a complex behavior that can possibly be elucidated through EIS.

Novel ARB characterizations

Our aim is to expand the library of novel ARB to be useful in number of applications. Consequently, our group decided to pursue the characterization of *Geoalkalibacter* in MXCs using some of the methods I have discussed. In some of the mixed community MXCs used in the microbial ecology study (Miceli et al., 2012) from our lab, we found an organism in the genus *Geoalkalibacter* as a putative ARB; however, there are also some previously isolated strains of this genus. Therefore, instead of isolating our very own strain of *Geoalkalibacter* from these reactors, we pursued characterizing these extensively microbiologically characterized strains, namely, *Geoalkalibacter ferrihydriticus* and *Geoalkalibacter subterraneus* (Greene et al., 2009; Zavarzina et al., 2006). As presented in these studies, these strains have a variety of electron donors/substrates, acceptors and different salinity as well as pH ranges (see the appendix A for the differences in both organisms) in which they can grow. Nevertheless, these strains have never been enriched in an MXC to produce current. We then conjectured that we should be able to use them as ARB based on their presence in MXCs in our enrichment studies. In addition, this genus is in close relationship to the genus *Geobacter* as determined by phylogenetic classification.

In embarking on this journey, these cultures, *Geoalkalibacter ferrihydriticus* DSM 17813 and *Geoalkalibacter subterraneus* DSM 23483, were obtained from the German Collection of Microorganisms and Cell Cultures (DSMZ). The cultures were maintained in culture tubes with the media suggested by DSMZ for each organism. We made glycerol stocks of these organisms, stored at -80 C, for later studies. Although each organism can use a variety of electron acceptors, we chose Fe(III) oxide simply because we have seen that cultures grown on amorphous iron oxide ultimately grow on the MXC anode. Fe(III) oxides are insoluble

electron acceptors, just like the anode, therefore, adapting them to grow on Fe(III) in culture tubes makes it easier to later grow them in an MXC. Badalamenti et al., (2013) focused on growing *Glk. ferrihydriticus* in MXCs and fully characterizing it using different electron donors, but also generated some preliminary results for G. *subterraneus*. From these studies, some thermodynamic and kinetic parameters were determined for *Geoalkalibacter ferrihydriticus* and it was also shown that this organism produces high current densities (up to 8 A/m^2). In the future, it may be possible that this organism rival *Geobacter* in the MXC community once it is fully characterized.

Using chronoamperometry, anodes in experiment were poised at -0.2V vs. Ag/AgCl with a potentiostat and the current was measured over time. *G. ferrihydriticus* produced current in MXCs under alkaline condition of pH 9.3 when fed 20mM acetate. The maximum current density recorded was 8.3 A/m^2 which similar to the values in the literature for *Geobacter sulfurreducens* (Katuri et al., 2012; Malvankar et al., 2012) at neutral pH. The substrate consumption was measured with HPLC and this revealed the Coulombic efficiency (percentage of electron donor being channeled to produce current) of *Glk. ferrihydriticus* to be 85-95% . With a small biofilm inoculum, the doubling time of *Glk. ferrihydriticus* was measured to be about 7.5 hrs. With 10mM ethanol as the electron donor, the maximum current density reported was 7.1 A/m^2 with an initial doubling time of 6.9 hrs. Initially, the maximum current density for the pure culture was much lower at 2.6 A/m^2 until Badalamenti et al., (2013) found acetate to be a byproduct of ethanol oxidation. Therefore, the higher number that was reported was after a media replacement, which provided further proof that ferrihydriticus consumed the ethanol and the acetate produced to generate the current. A CE of approximately 95% was also recorded for ethanol oxidation in this MXC.

To determine *Glk. ferrihydriticus* respiration kinetics, cyclic voltammetry was carried out at low scan rates; thereby, allowing the biofilms to reach steady-state. CVs generated when acetate was fed showed a sigmoidal wave indicative of redox processes taking place. The midpoint potential was recorded to be -0.21V vs. SHE, a potential 60mV lower than the accepted midpoint potential (-0.15 V vs. SHE) for *Geobacter sulfurreducens* (at neutral pH) in the literature. This study suggests that due to the low open circuit potential (potential at which no current is being generated) of -0.37 V vs. SHE recorded for *Glk. ferrihydriticus* and the two-pH units difference, it is sensible that the midpoint potential be what was reported. With ethanol-fed biofilms the shapes of the sigmoidal CVs generated were identical to that generated from acetate fed biofilms; giving the same midpoint potential. The difference lies in their open circuit potentials. As reported in this study, the open circuit potential was -0.41 V vs. SHE, which was not surprising considering that ethanol is a more reduced substrate than acetate.

The authors also investigated Glk. *subterraneus* as a good comparison to *Glk. ferrihydriticus* showing the differences between the two organisms. For example, *Glk. subterraneus* grown on acetate produces lower current than its counterpart (~2 A/m^2). It also has a midpoint potential and open circuit potential of -0.19V vs. SHE and -0.28V vs. SHE respectively. CVs at the early growth stages (first week) show multiple redox peaks at different potentials a few hundred millivolts around the midpoint potential, but these peaks later disappear in the CVs generated with a matured biofilm. There are glaring differences in both *Geoalkalibacter* species with *Glk. ferrihydriticus* preferring the alkaline pH and *Glk. subterraneus* preferring neutral pH with a high saline media. *Glk. Subterraneus* also seems to be non-discriminatory in its electron donors from acetate to propionate to glycerol and even

stearate, but we are unsure of how it will behave in an MXC with this variety of reduced organics at this point.

I continued the investigation of *Glk. subterraneus* in an MXC using acetate, butyrate and glycerol as the electron donors (Chapter 5). In the coming chapters, these experiments will be discussed in further detail while providing parameters we were able to determine from our study.

CHAPTER 3

MATERIALS AND METHODS

MXC construction, Operation and inoculation

- For EIS experiments (Chapter 4)

We made use of 100 mL glassware with an opening on the side for a 2 mm diameter gold anode (CH instruments, CH101). We drilled holes in rubber stoppers for the media lines and a thin platinum cathode. This apparatus is sterilized by autoclaving at 121^0C with a 30-minute sterilization time. Upon cooling, an Ag/AgCl reference electrode (BASi, West Lafayette, IN) is dipped in 70% ethanol, flicked dry, and carefully inserted into the rubber stopper. The reactor is then filled in a biosafety cabinet by flowing nitrogen-pressurized media through sterile Norprene tubing (Cole Parmer, Vernon Hills IL). The reactor is sparged with 0.22 μm filtered 80% N2: 20% CO2 gas mix for 30 minutes. The reactor was constantly agitated with magnetic stirring.

Inoculum was always 1 mL of pure *Geobacter sulfurreducens* isolate from an enrichment reactor.

- For *Glk. subterraneus* donor experiments (Chapter 4)

We constructed dual-chamber H-type MECs (350 ml anode volume) with two graphite rod anodes (5.27cm^2 total area) and sterilized them by autoclaving. We polished those graphite anodes to a smooth surface by sanding with 600-grit followed by 1,500-grit aluminum oxide-silicon carbide sandpaper (McMaster-Carr). Pieces of anion exchange membrane (AMI 7001; Membranes International, Inc.) were autoclaved while soaked in 3 M NaCl and inserted into the autoclaved assembled MEC. An Ag/AgCl reference electrode (BASi, West Lafayette, IN) was dipped in 70% ethanol, flicked dry, and inserted into anode chambers. The cathode contained a sterile, anoxic 2% NaCl solution adjusted to pH 12.5

with 10M NaOH. Reactors were also filled as previously stated above. Before inoculation, cathodes were sparged with N_2 and anodes with filtered (0.22 μm pore size) 80%N_2: 20%CO_2 gas. Anode chambers were agitated constantly at 150 rpm by magnetic stirring. As previously reported in Badalamenti et al 2013, to promote utilization of anodes as electron acceptors, *Geoalkalibacter* cells were cultured in medium containing 50 mM Fe(III) oxide, and 3 ml of these cultures were used to inoculate MECs. To inoculate subsequent growth experiments, we scraped a small biofilm section using a needle into 1 ml sterile medium in an anaerobic chamber (Coy Laboratory Products, Grass Lake, MI) and used 0.1 ml of this cell suspension as the inoculum. Media replacements were performed in the anaerobic chamber by transferring the anode and reference electrode to a clean MEC containing sterile medium.

Chronoamperometry and Cyclic voltammetry

- Cyclic Voltammograms (CVs)

Anode was poised at -0.3V vs. Ag/AgCl as previously described (Badalamenti et al., 2013). Using a window of -0.48 V and 0.2 V, CVs were collected after the anode has reached open circuit potential at the early stage of growth and at saturation. The scans started at the upper limit down to the lower limit of the potential window. Midpoint potentials were determined from these plots. For *Glk. subterraneus* growth experiments, anodes were poised at -0.2V vs. Ag/AgCl (-0.04V vs. SHE) using the VMP3 potentiostat as previously described (Badalamenti et al., 2013). Using a window of -0.6V and 0.1V, cyclic voltammograms were obtained here early and later in growth period. The channel on the potentiostat was stopped and the anode is allowed sufficient time to reach open circuit. The scan starts at open circuit towards the upper limit of the set potential window and back to the lower limit. Midpoint

potential was obtained for this organism during growth the three different substrates investigated.

- Electrochemical Impedance Spectroscopy

EIS measurements were done as a function of growth for *Geobacter sulfurreducens.* At 0.5 A/m^2, 1 A/m^2, 2 A/m^2, 3 A/m^2, 4 A/m^2 and saturation, measurements were taken at two different potentials, -0.3V and -0.39V vs. Ag/AgCl. The first potential is the potential at which *G. sulfurreducens* was grown at and the second is close to the midpoint potential determined by the CVs. A few measurements were performed between these specified current densities when we notice a change in growth pattern (i.e, pseudo-saturation). Also, I took two measurements at saturation separated by approximately a day. The method used for these measurements has an equilibration time of 15 mins at each potential, amplitude of 15 mV and a frequency range of 200 kHz to 50 mHz.

To generate the resistance vs. potential graphs, EIS measurements were obtained for *G. sulfurreducens* every 20 mV between the range of -0.5V and -0.25V vs. Ag/AgCl once the biofilm has reached saturation (j_{max}). For *Glk. subterraneus*, EIS measurements were done also at saturation every 25mV between the range of -0.55V and -0.3V vs. Ag/AgCl once the biofilm has reached saturation. The range of potentials was determined by the CVs done before the EIS experiments. The CVs give us an idea of where the linear regions and the exponential phases are so as to truly capture all aspects of the changes in resistance in our MXCs.

- HPLC Methods

As previously reported in Parameswaran et al., 2009, samples are analyzed using high-performance liquid chromatography (HPLC; Model LC-20AT, Shimadzu,

Columbia, MD): acetate, butyrate, and glycerol consumption could be analyzed in the samples. An Aminex HPX-87H (Bio-Rad Laboratories, Hercules, CA, 1997) column separated the simple acids and alcohols, sulfuric acid at 2.5 mM was the eluent fed at a flow rate of 0.6 mL/min, and chromatographic peaks were detected using photo-diode array (210 nm) and refractive index detectors. The total elution time was 50 min, and the oven temperature was constant at 308°C. We developed a calibration curve for every set of analyses, performed duplicate assays, and report average concentrations.

- Coulombic efficiency (CE) measurements

A 0.5 mL sample of inoculum was filtered into an HPLC vial as well as 1 mL of filtered *Glk subterraneus* media with substrate as the time zero sample. After a sufficient amount of charge has been collected from the donor, a few more samples are collected within a few days of each other. These samples are analyzed using the HPLC along with a standard of substrates indicative of different concentrations that could be present in each sample collected. From the HPLC data of concentrations and the recorded charge measurements at the time of sampling, the Coulombic efficiency is calculated using this equation: $CE = \frac{\Delta dQ\ (recorded)}{\Delta mmol * n * F}$. Here, *total Q* refers to the total charge available per substrate (butyrate, acetate or glycerol) and $\Delta mmol$ refers to the difference in mmol of substrate in each sample.

- Electron acceptor preparations

I used 50 mM-amorphous Fe (III) Oxide as the acceptor for *Glk. subterraneus* growth experiments. Specifically, we pre-adapted the cells to growing on this acceptor before we grew them on an MXC anode. We prepared a 1 M stock solution as follows:
We dissolved 13.52 g $FeCl_3$ x $6H_2O$ in 125 mL deionized water for a final concentration of 0.4 M. The solution was continually agitated while adjusting the pH to 7.0 with 10 M NaOH solution being careful not to allow the pH to rise above 7 at anytime during this preparation. We continued to stir for 30 mins after the pH had stabilized at 7, but adjusted the pH as needed. We then centrifuged the suspension at 4000 x g for 3 mins, discarded the supernatant and re-suspended the rest in water, then centrifuged again. This process was repeated 3 times until the iron oxide is re-suspended to a final volume of 45mL and transferred into a sterile 125 mL serum bottle. Once sealed, the content of the serum bottle was sparged with N_2 gas for at least an hour and autoclaved for at least 20 mins at 121°C.

- Media Preparations

<u>*Geobacter* EIS experiments</u>

We used media with 10mM acetate and 30mM sodium bicarbonate prepared as follows: Sequentially, the following chemicals namely, 1.5 g (28 mM) of NH_4Cl, 0.60 g (4 mM) of NaH_2PO_4, 0.10 g (1 mM) of KCl, 1.36 g (10 mM) of sodium acetate trihydrate, and 10 mL of Trace Minerals **are dissolved in deionized water to total of 960 mL and autoclaved for at least 20 mins at 121°C. Once cooled, 30 mL of 1 M Sodium Bicarbonate was added aseptically to the media along with 10 mL of ATCC Vitamins. The completed media was then bubbled with 80% N_2: 20% CO_2 gas mix for approximately 45 minutes.

**Trace mineral mix was prepared as follows in 1L of water:

1.5 g of Nitrilotriacetic acid (trisodium salt), 3.0 g of magnesium sulfate heptahydrate ($MgSO_4$ x 7 H_20), 0.5 g of manganese sulfate monohydrate ($MnSO_4$ x H_20), 1.0 g of sodium chloride (NaCl), 0.1 g of iron sulfate heptahydrate ($FeSO_4$ x 7 H_20), 0.1 g of calcium chloride dihydrate ($CaCl_2$ x 2 H_20), 0.1 g of cobalt chloride hexahydrate ($CoCl_2$ x 6 H_20), 0.13 g of zinc chloride ($ZnCl_2$), 10 mg of copper sulfate pentahydrate ($CuSO_4$ x 5 H_20), 10 mg of $AlK(SO_4)_2$ x 12 H_20, 10 mg of H_3BO_4, 2.5 mg of Na_2Mo0_4 x 2 H_20, 2.4 mg of nickel chloride hexahydrate ($NiCl_2$ x 6 H_20), and 0.25 mg of Na_2W0_4 x 2 H_20 were added to 1L of water. The solution was then transferred to a media bottle aseptically and stored at 4^0C.

For *Glk. subterraneus* experiments

42 mM Bicarbonate *Glk. subterraneus* (donor free media) was made by dissolving the following materials:

17 g of sodium chloride (NaCl), 4.50 g of magnesium chloride hexahydrate (MgCl x 6 H_20), 0.35 g of calcium chloride dihydrate (CaCl x 2 H_20), 1 g of ammonium chloride (NH_4Cl), 80 mg of monobasic potassium phosphate (KH_2PO_4), 3.0 mL of trace mineral solution* and 0.5 mL of Selenite-Tungstate solution *.

In a graduated cylinder with deionized water, the mixture was brought to a total 948mL and autoclaved for at least 20 mins at 121°C. Then, once cooled, 42mL of a 1 M Sodium Bicarbonate stock and 10mL of ATCC Vitamins were added. The solution was bubbled with 80% N_2: 20% CO_2 mix for 45mins before using.

*Trace mineral solution protocol

In 1 L of deionized water, the following compounds were dissolved and thoroughly mixed in the following order:

12.5 mL of 25% hydrochloric acid (HCl; 7.7M), 2.1 g of iron sulfate heptahydrate ($FeSO_4$ x 7 H_20), 30mg of boric acid (H_3BO_3), 0.1 g of manganese chloride tetrahydrate ($MnCl_2$ x 4 H_20), 0.190 g of cobalt chloride hexahydrate ($CoCl_2$ x 6 H_20),

24 mg of nickel chloride hexahydrate ($NiCl_2$ x 6 H_20), 2 mg of copper chloride ($CuCl_2$ x 2 H_20), 0.144 g of zinc sulfate heptahydrate ($ZnSO_4$ x 7 H_20), and 36 mg of Na_2Mo0_4 x 2 H_20. This was done aseptically and consequently stored at 4^0C.

*Selenite Tungstate solution:

In 1 liter of DI water, 0.5 g NaOH was dissolved and the following were added sequentially: 6 mg sodium selenite (Na_2SeO_3 x 5 H_2O) and 8 mg sodium tungstate (Na_2WO_4 x 2 H_2O).

Sodium Bicarbonate solution:

1 M stock was prepared by adding the appropriate amount (10.5 g) into 125 mL of deionized water. Once completely dissolved, the solution was bubbled with the 80% nitrogen/ 20% carbon dioxide gas mix for approximately 45 mins, then transferred into a serum bottle in the anaerobic glove box. The headspace was exchanged with the same gas mix and the solution is autoclaved for at least 20 mins at 121°C.

Preparation of donors:

1 M stock of each donor was prepared in a graduated cylinder by dissolving the appropriate amount of Sodium acetate trihydrate, Sodium butyrate or glycerol into 125 mL of deionized water. Once dissolved and thoroughly mixed, the mixture was transferred into a small media bottle and bubbled with Nitrogen until anaerobic (~45 mins). Along with butyl rubber stoppers, caps, a crimper and 125-mL serum bottles, the bottle containing each donor was taken to the anaerobic glove box where the contents were transferred to the serum bottles, capped and crimped. The headspace of each serum bottles containing donor was replaced with nitrogen and autoclaved for at least 20 mins at 121°C. Typically, these were added into reactors while filling them to a final concentration of 20 mM, 5 mM and 10 mM of acetate, butyrate and glycerol respectively.

Counter Chamber Solution:

In a graduated cylinder, 20 g of NaCl was dissolved into deionized water and fill the cylinder close to 1 L. Concentrated NaOH was added dropwise until the pH reached 12.5; being careful not to overshoot past pH 12.5. Then, water was added to exactly 1L while making sure the pH remains at 12.5. The contents were transferred into a 1 L bottle and autoclaved for at least 20 mins at 121°C. After the solution was cooled, it was bubbled with nitrogen gas for approximately 45 mins to make it anaerobic.

CHAPTER 4

ELECTROCHEMICAL IMPEDANCE SPECTROSCOPY – RESULTS AND DISCUSSION

The underlying objective of the EIS study on *Geobacter* is to determine if extracellular electron transfer (EET) resistances in the ARB biofilm are rate-limiting. For this purpose, we used measurements obtained as a function of growth and followed how resistances behave as the biofilm grows and the EET distance increases. We hypothesized that as the biofilm grows, the increase in EET-active proteins (e.g., cytochromes) will affect the resistances and the capacitances in the system. Once the biofilm is fully grown, both capacitances and resistances should stabilize. Because our system is modeled after a simple Randles circuit, we anticipate that in the range of frequencies we have chosen for our measurements, the Ohmic resistance measured should not be changing (if the EET mechanism is primarily Nernstian in nature). On our Bode and Nyquist plots, we are able to differentiate between different processes taking place and the resistances corresponding to each process can be obtained via an analysis method, Z-fit. These resistances and capacitances are normalized by surface area and by the calculated biofilm thickness, as determined by Robuschi et al., 2012. CVs were also performed at various growth stages and fitted to the Nernst-Monod model.

The motivation for growth experiments came from our previous studies on *Geobacter,* where we obtained resistances as a function of anode potential[1]. In this study, we performed EIS measurements at potentials that are 20mV apart. For each charge transfer process present; we graphed the resistances vs. anode potential. This plot is representative of the

[1] The experiments related to Figures 4.1 and 4.3 were led by Dr. Sudeep Popat and assisted by Rachel A.Yoho and myself.

total resistance in the system. We used the unique combination of CVs and EIS because although they are different methods, there exists an important correlation between the two. With the Nernst-Monod equation, we can generate the current/potential sigmoidal response typical of *G. sulfurreducens* biofilms. In Figure 4.1a, we plot j/j_{max} according to the Nernst-Monod equation with an $E_{KA} = 0$ using the range of potentials specified as the value of E. We used two values for n in order to show the differences in the plots with this parametric change. According to Ohm's Law, V = iR, it is evident that the slope of a CV is the inverse of resistance. Since EIS gives us the resistance information, we plot on Figure 4.1b the inverse of the slope of the sigmoidal CV curve in order to get the expected shape of the resistance vs. potential curve. I will refer to this curve as the U-shape curve throughout the document; this U shape is specific to the Nernst-Monod's sigmoidal behavior. While increasing values of n translates into increasing slope of the CV, it translates into the narrowing of the U-shaped curve.

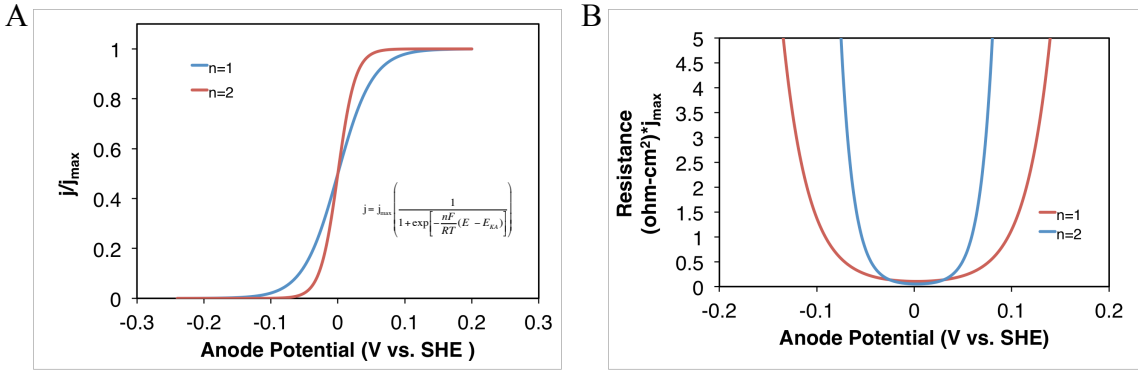

Figure 4.1. (A.) Two Nernst-Monod CVs generated with E_{KA} of 0 and j_{max} of 1 to show the effects of changing the value of n. The Nernst-Monod equation is displayed on the graph. (B.) The corresponding resistance vs. potential graph in the linear region of the CVs plotted in A. The resistances were calculated by taking the inverse of the slope of the linear region, which happens to be 1/R.

Therefore, with every EIS measurement set, we expected a U-shape relationship between resistance and potential, indicative of a microbial/enzymatic process. As a sigmoidal curve has been deemed to be a characteristic of an enzymatic process, so is the U-shape curve with its minima representing the midpoint potential of a particular enzyme. However, in our EIS experiments with *G. sulfurreducens*, we consistently generated a double U curve, suggesting that there must be more than one pathway for electron transfer, each with a distinct rate-limiting protein being expressed (Figure 4.3a). The relationship obtained suggests there are two midpoint potentials (E_{KA}) corresponding to two different proteins. One of the E_{KA}'s is closer to the potential at which the bacteria are grown, -0.02V and the other is more negative.

As expected, a CV of the same biofilm (Figure 4.3b) cannot be fitted with a single Nernst-Monod curve; the CVs always show two inflections (Figure 4.3b), indicative of two possible redox processes occurring in parallel. When using a Nernst-Monod fitting for two governing protein in parallel, we were able to fit both EIS and CV data, as shown in Figure 4.3b. This confirms that the two processes observed are in parallel, that is, there are at least two different pathways that operate in parallel.

As a comparison to *Geobacter*, I also decided to do EIS measurements on our halophilic ARB, *Glk. subterraneus*. The purpose of these measurements is to compare the processes governing electron transfer. I decided to do same EIS experiments as a function of anode potential that produce the double U responses for *Geobacter*. *Glk. subterraneus* is grown at 0.04V vs SHE (standard potential to grow these in our laboratory). There are key differences between these two organisms physiologically as we have previously discussed,

but there are also similarities. Rather than two redox processes (double U), I observe three redox processes (Figure 4.2).

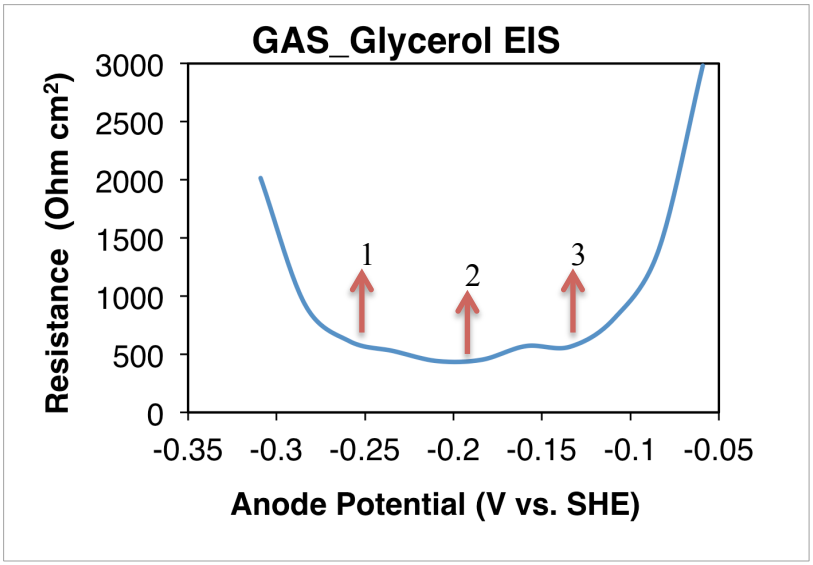

Figure 4.2. EIS resistance vs. anode potential graph for *Glk.subterraneus* macroscopically showing three redox processes (triple U-response) in parallel as indicated with arrows.

This data can later help us in understanding the electron-transfer resistances in *Glk. subterraneus* since the first report of it functioning as an ARB is rather recent (Badalamenti et al., 2013). Since reasonable current densities are generated, understanding its EET mechanism will provide a great insight into a promising organism in the applications associated with MXCs.

We hypothesized that ARB cells change their preferred transport protein depending on their position in the biofilm. How does it change expression of its mechanism of electron transport? Is this a function of a potential gradient inside the biofilm? Herein lies our motivation to perform growth experiment. We hypothesized that CVs done at different growth stages (Figure 4.4) will illuminate the potential gradient we think exists in our system. We decided to do CVs mainly because they are faster to obtain than EIS measurements. To

do EIS measurements that can give the same information will require us interrupting the system for close to 2 hrs at a time because each potential takes 10 minutes, and to capture the whole range, I will have to take measurements at 10-12 potentials. This length of time is considerably longer compared to approximately 30 min it takes to generate a CV. We did not completely exclude EIS because we performed EIS experiments at various growth stages to elucidate the underlying mechanisms that are changing as a function of biofilm growth. However, we chose only two representative potentials for these experiments, growth potential and a potential closest to the midpoint as indicated by CVs.

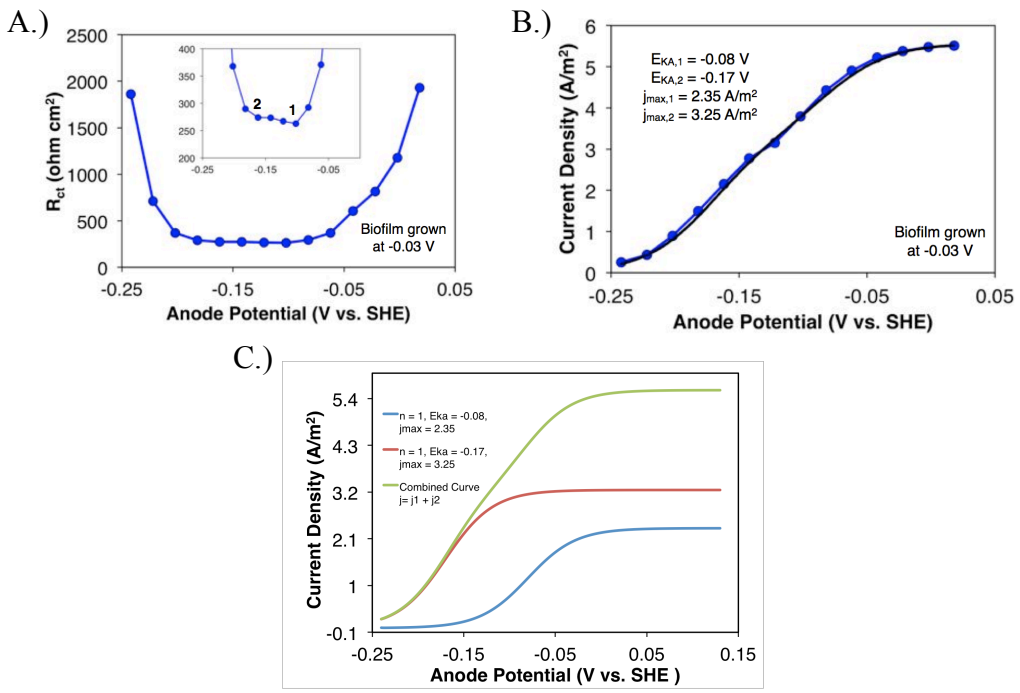

Figure 4.3. (A.) Resistance vs. anode potential graph macroscopically showing the U-shape expected from this analysis. A zoomed in version shows the double U response with the two E_{KA} values marked as 1 and 2. (B.) Our experimental data for a fully-grown *G. sulfurreducens* biofilm in blue fits the N-M model with two parallel processes shown in black. (C.) A representation of how two n=1 transfer processes in parallel changes the apparent n value to a value less than one (data not yet published).

The CVs as a function of biofilm growth were obtained at 0.5A/m^2, 2A/m^2 and at saturation (4.8 to 5 A/m^2), as shown in Figure 4.5. All CVs are sigmoidal with changing shape as a function of growth (Figure 4.5). The CV's midpoint potential becomes more negative as the biofilm grows. The change in the CV shapes is represented in figure 4.5B where CVs at the lowest and the highest current densities are reported as j/j_{max}. These normalized CVs make the change obvious. The changes observed are consistent with a biofilm potential gradient. The young biofilm (0.5 A/m^2) generates a high-potential signal

(E_{KA} = -0.08 V) with a n=2 Nernst-Monod fit. However, the older biofilm shows a mixed Nernst-Monod fit that also includes a lower potential signal (E_{KA} = -0.17 V). We hypothesize that as the biofilm grows, a potential gradient then exists for the cells further from the electrode that still need to make contact with the electrode. For the ARB to now overcome this gradient, the bacteria farther away from the anode must switch from one protein/cytochrome in the EET pathway to the other with lower E_{KA}. This shift is clearly detrimental to their ability to harvest energy from anode respiration, since they lose ~90 mV by using the more negative electron-transfer process.

This change in the CV shape supports what we have noticed with the double U response of resistance vs. potential curves from our earlier EIS experiments (Figure 4.3a). Additionally, the N-M fit for each of the CVs obtained revealed the changes in the value of n as well. At the lowest current density corresponding to having a thin biofilm, the value of n is larger than one and at saturation. This translates to a change in the slope of the CVs. When n>1, the slope is steeper than n=1, and when n<1, the slope is broader than n=1, but as shown in Figure 4.5b, n = 1 does not fit the data as well as we have seen in our previous experiments. This once again suggests that the EET process is more complicated than what we imagine it to be. The parallel processes discussed above could explain the CV observations.

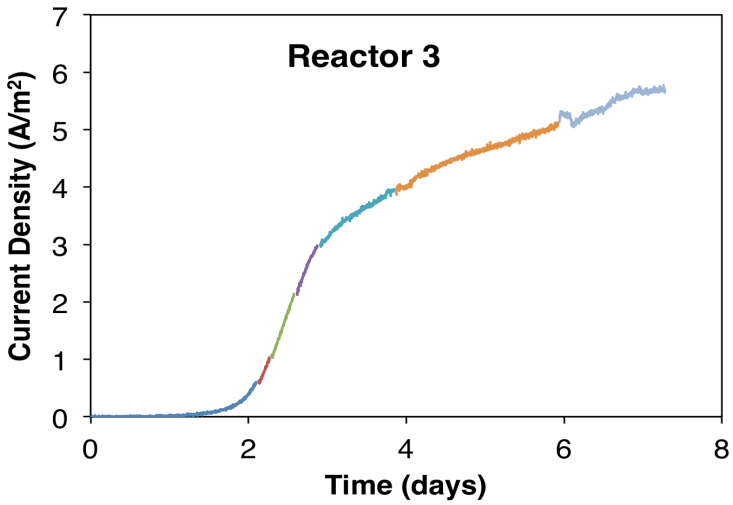

Figure 4.4. The growth curve of 10mM acetate fed *Geobacter* obtained from the third replicate. EIS was performed at the end of each color segment of the growth curve.

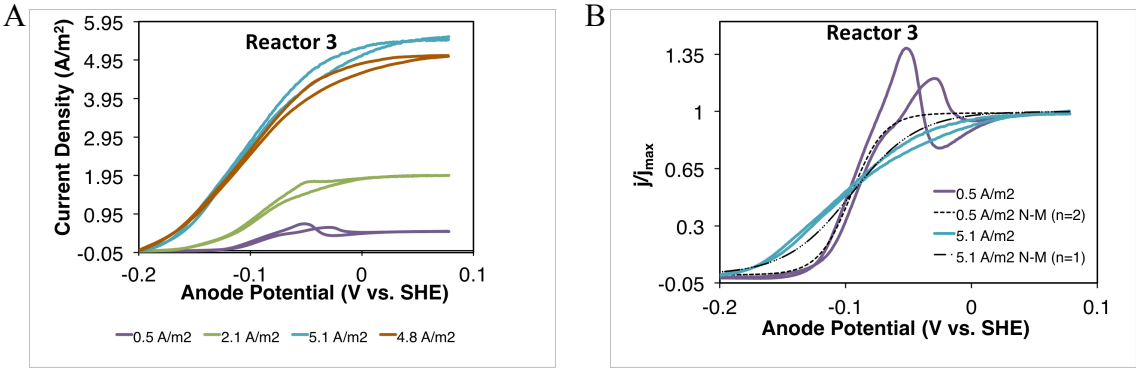

Figure 4.5. (A) CVs done as a function of growth. As the biofilm grew, the shapes of CVs changed. (B) CVs obtained when the biofilm was the thinnest (0.5 A/m^2) and also thickest (5.1 A/m^2) represented as j/j_{max} to show the obvious change in the CVs. As the biofilm became thicker, the CVs become smoother as well. The N-M fits are also shown here in black dotted lines and the E_{KA} shifts slightly to a more negative potential.

At this junction, I reason that the potential at which we are growing the bacteria has much to do with the results we are obtaining. To confirm this hypothesis on the potential gradients causing a shift in expression of the protein/cytochrome in the EET pathway, experiments are underway to grow the bacteria at a lower potential comparable to the potential at which *Geobacter* has been previously grown in Torres et al., 2008 (-0.13 V vs SHE). We predict that at this lower potential, the resistance vs. potential curve will give a U response and not a double U response simply because there may only be one of those EET protein(s)/ cytochrome(s) preferred for the bacteria. Thereby, only one pathway will be predominant.

Geobacter EIS results

From the data presented above, we can conclude that there is more than one pathway responsible for the electron transfer. In order to elucidate the processes responsible for the phenomenon we are discovering at -0.02V growth potential, we performed EIS measurements also as a function of growth and as a function of potential. By so doing, we expected to be able to tease out the individual resistances in the system and use them to gain a better understanding of the potential gradients we see. Through EIS, we also expected to gain a deeper understanding towards the EET mechanism of *Geobacter* as it has constantly been a subject of contention.

From the data collected in these experiments, we could clearly distinguish three resistances at work; an Ohmic resistance (R1) and two charge transfer resistances (R2 and R3). An example of such plots is shown in Figure 4.6 with the resistances labeled. All experiments presented were repeated at least three times and the results are similar. Here, I

will report our data from my third replicate (Reactor 3), but the other data are made available in the appendices.

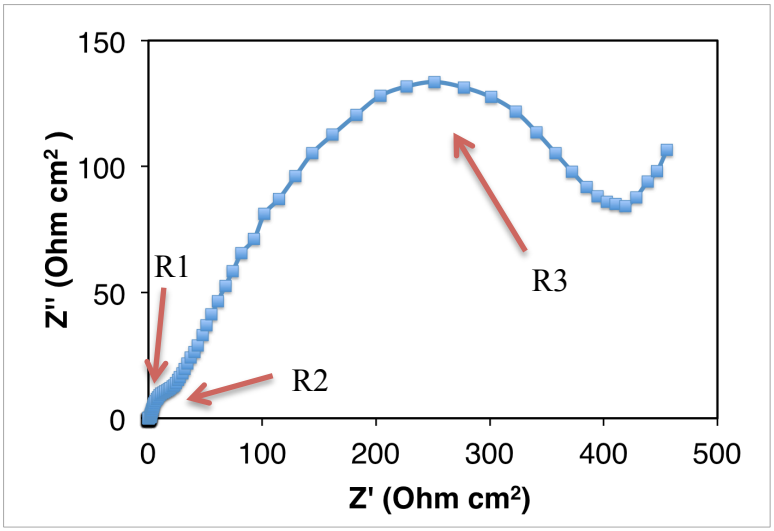

Figure 4.6. An example of Nyquist plots we generate showing the resistances we refer to as ohmic (R1), the first corresponding value on the x-axis, and the charge transfer resistances (R2 and R3), the later values once extrapolated onto the x-axis. The x-axis shows the real impedance values that are reported.

One school of thought on the EET mechanism of *Geobacter* claims that the "nanowires" act as metallic-like conductors (Malvankar et al., 2011; Malvankar et al., 2012). If true, the Ohmic resistance should increase as the biofilm grows due to the presence of the nanowire resistance within the biofilm. However, if the nanowire resistance is Nernstian in nature (electron hopping through cytochromes), the Ohmic resistance should not change significantly as the biofilm grows; instead, other Nernstian resistances (U-shapes) should increase. We observe an increase in Ohmic resistance, R1, within the error range of EIS measurements. However, as shown in Figure 4.7 this resistance does not increase significantly.

The Ohmic resistance has two components, the electronic (R_{elec}) and the ionic component (R_{ionic}) (O'hayre et al., 2009). The electronic resistance comes from the path of electrons through electrodes, connections to electrodes, and possibly through nanowires. However, the majority of the Ohmic resistance comes from R_{ionic} because of the ionic transport in the electrolyte, between the anode and the reference electrode.

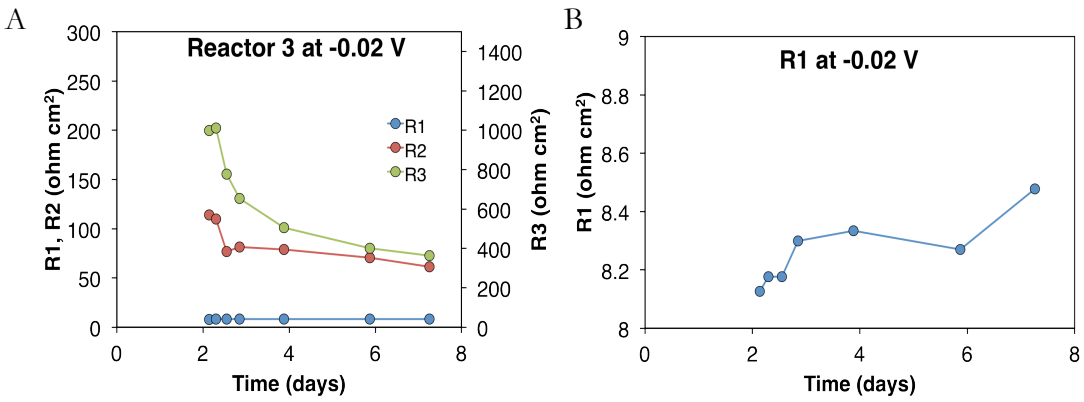

Figure 4.7. (A.) All resistances (ohm cm^2) vs. time plots obtained from EIS measurements obtained at -0.02V vs. SHE. (B.) Zoomed in plot of Ohmic resistance at the same potential shows slight increase in this resistance.

In a young biofilm, R_{ionic} is the main Ohmic loss. The increase in Ohmic resistance as the biofilm grows could be the result of a "nanowire resistance". However, an increase in R_{ionic} is also expected because the biofilm presents an added layer of ionic resistance due to the tortuosity of the ionic path between electrodes. As the biofilm grows, the distance from the electrode remains the same, but the ions no longer have a clear path. The cells that have now colonized the electrode amount to a significant hindrance to ion transport. Thus, we cannot conclude from these results that we can quantify a "nanowire" Ohmic resistance. However, we can conclude that, if nanowires are indeed acting as Ohmic resistors, their conductivity is very high and they impart a negligible resistance to the biofilm system. This

is obviously not consistent with our previous results that suggest there is a biofilm potential gradient due to EET resistances.

Although this is an important discussion, this work will not focus on the Ohmic increase because evidently, other resistances play a much larger role in our system. The other two resistances we see when we analyzed our EIS data are about 100 to 300 times larger than the Ohmic resistance as shown in Figure 4.8a. It is then safe to assume that the processes represented by these resistances dominate the limiting electron-transfer kinetics of our *Geobacter* strain.

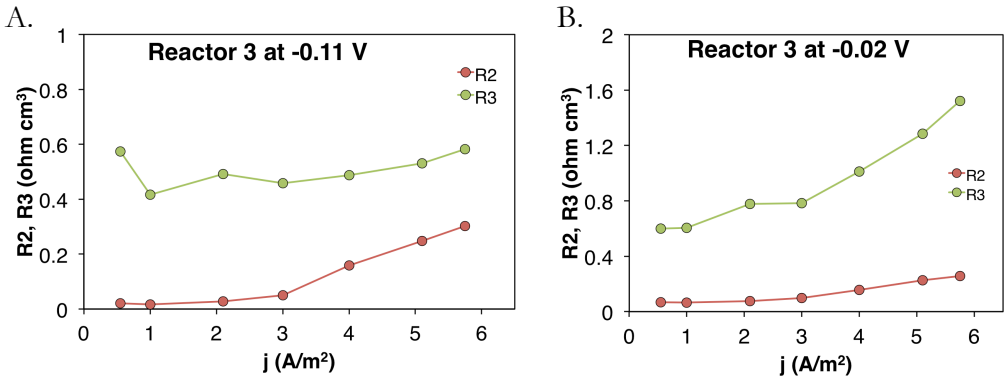

Figure 4.8: Charge resistance measurements at both potentials at which EIS measurements were obtained.

All our EIS data was collected as total resistance (Ohm) and normalized per the surface area (Ohm cm^2). However, in order to better discuss the effect of biofilm growth on the resistances observed, we normalized our data with biofilm volume (Ohm cm^3) using values reported in literature from a study that established the relationship between current density and biofilm thickness for *G. sulfurreducens* (Robuschi et al., 2012). From this study, I extrapolated approximate corresponding biofilm thickness measurements (Table 1.1).

Table 4.1: Relationship between current density and biofilm thickness for *G. sulfurreducens*

Adapted from the following reference: Luciana Robuschi et al., (2012)

Current Density (A/m^2)	**0.5**	**0.55**	**1**	**1.2**	**2.1**	**3**	**3.55**	**4**	**4.7**	**5**	**5.1**	**5.7**	**5.8**	**6.1**
Biofilm thickness (μm)	6	6	6	7	10	12	14	20	28	30	32	42	42	57

It became more glaring that one of these charge resistances, R3, is playing an even bigger role, as it is larger than the other. Since the biofilm grows in layers, we can think of resistance in terms of biofilm thickness. The normalization to biofilm thickness presumes that at every layer of growth, there should be the same cellular machinery accumulated. Even more interestingly, R3 does not behave the same way at the two potentials where measurements were taken. At -0.02V (the growth potential), R3 continues to increase even at saturation (Fig 4.8b) while at -0.11V, closer to the E_{KA}, R3 remains rather constant, but still bigger than R2 (Fig 4.8a). Further studies need to be conducted to shed light on the details of these results, especially in terms of what pathway this could be representing. Since we do not delve into the realm of proteomics or protein film voltammetry, it is impossible to make any conclusions as to what component of the cell is causing the most resistance to electron transfer. To this end, however, there have been studies that sought to make these inferences. It has been proposed that a periplasmic protein is the one responsible for the biggest resistance (Pessanha et al., 2006) and an outer membrane cytochrome responsible for the second charge transfer resistance (Qian et al., 2011). While we did not seek to validate these findings, we can say that the behavior of R3 at both potentials is important. According to the CVs we have shown thus far, -0.02V corresponds to the saturation potential of our *Geobacter*

strain. The increase in R3 suggests that there is a limitation to the growth of the bacteria. *Geobacter* has been shown to grow to current densities close to 8 A/m^2 (Yi et al., 2009), and even up to 10 A/m^2 in a mixed consortium (Parameswaran et al., 2011), but we have not seen that in these experiments. We know that there must be some limitations to reaching higher current densities at the conditions of growth we specified for this strain. From our results, we know the resistance responsible for this limitation is R3. At the attachment phase, the cells are still growing and there is not any limitation to growth, hence this resistance is constant for the most part.

Being that a circuit models our system, the next part of the circuit that we can measure from our EIS measurement is the capacitance. These values were also normalized by the predicted biofilm thickness from literature. We reason that the capacitance is a function of the redox-active proteins present in the system; thus, the normalized capacitance should increase as the first monolayer of cells attach to the electrode. However, we presumed that redox-active proteins are more densely packed closer to the anode. From the perspective of the bacteria, there is an inherent gradient as it relates to the availability of electron acceptor, as the distance to the electrode gets larger. Hence, the cells at the topmost layer of the biofilm do not benefit from making more cytochromes. Consequently, as the biofilm grows, the normalized capacitance should decrease. In fact, this is what we observe. Because there are two charge-transfer resistances, there is a corresponding capacitance for each resistance. In Figure 4.9, I show this increase in capacitance per cubic centimeter from measurements taken at 0.5 A/m^2 and 1 A/m^2. This is indicative of the first layer of cells. Subsequent capacitance measurements continue to go down as we have hypothesized. This

is observed at both -0.02V and -0.11V, but with no real difference between the rates of decrease at both potentials.

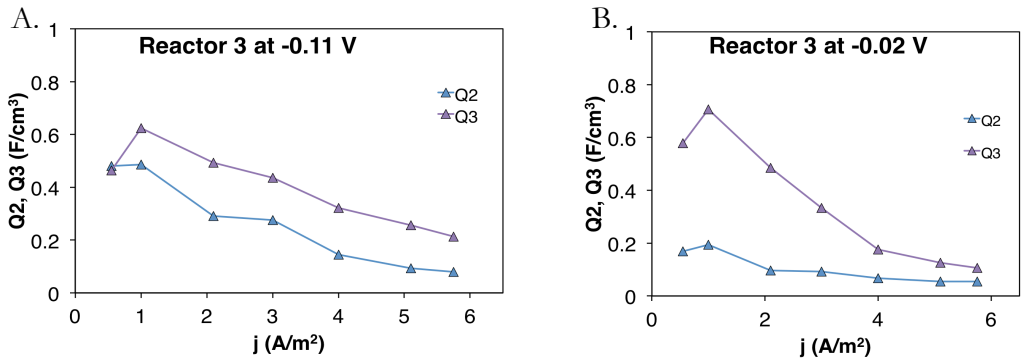

Figure 4.9. Capacitance measurements at both potentials at which EIS measurements were obtained.

Summary and Concluding Remarks

In the journey to understand the electron-transfer processes of *Geobacter*, we have discovered from our data that the simple N-M fit with n being 1 reported in literature does not match the actual electron-transfer phenomena. The process is not governed simply by one n =1 step, but rather a few processes in parallel with one primarily having the biggest impact. Additionally, the Ohmic resistance does not contribute significantly to the total biofilm resistance. This has led us to conclude that the EET mechanism that *Geobacter* exploits is more long-range electron transfer by the help of redox-active proteins participating in the electron hopping process (Strycharz-Glaven and Tender, 2012). We have also learned that the potential at which the bacteria are grown is crucial as the cells can minimize potential losses by using the most favorable pathway for electron transport. This is supported by the potential gradient we see in the CVs done at the different growth stages at which evaluation and EIS measurements were carried out. Obviously, our results stress the

need to further understand *Geobacter's* EET and this topic will continue to be a subject of discourse in the MXC community.

CHAPTER 5

GEOALKALIBACTER SUBTERRANEUS CHARACTERIZATION RESULTS AND DISCUSSION

My second goal was to characterize a novel ARB, *Glk.subterraneus* that might have unique capabilities for MXC applications. Earlier, it was discussed that in some of our saltwater enrichments, the genus *Geoalkalibacter* was present. In order to further understand these putative ARB, we studied two pure cultures that have been already microbiologically characterized. In the recent publication by Badalamenti et al, (2013), the authors discussed their efforts to characterize *Glk. ferrihydriticus* as an ARB. In this study, this organism was fed acetate and ethanol and the Coulombic efficiencies for both substrates and the current densities rival that of *Geobacter* in an MEC (Chapter 2). We now have the task of uncovering what substrates *Glk. subterraneus* can utilize when coupled to the anode respiration. Although, there is a long list of potential electron donors from which we can choose, not all are ideal for MXC use. For example, there are donors like stearate and palmitate that have low solubility because of their high molecular weight due to their longer hydrocarbon chains. Thus, we envisaged that these fundamental studies would be difficult to carry out if we were to use them.

With this in mind, I ventured to compare the growth and electrochemical behavior of *Glk. subterraneus* using acetate and also two other more reduced compounds, butyrate and glycerol. Apart from the fact that this choice of donors provides a sample of types of compounds, simple acids to alcohol to longer chains, they are also significant in fermentation and the industrial MXC applications. Butyrate is oftentimes a dead end fermentation product and it will be beneficial to find an ARB to consume it directly (Torres

et al., 2007). Since it is a four-carbon compound with potentially more electrons for use, the consumption of butyrate from a fermentation effluent is essential to achieve a high CE. Also, butyrate has been used in our lab in the past, but in a mixed consortium (Miceli, personal communication). Therefore, butyrate as a donor for a pure culture MEC will be a feat.

Glycerol on the other hand was chosen for a few different reasons; it is inexpensive, but most importantly it has a significance in the biodiesel industry. The process of taking animal oils and vegetable oils and converting them to biodiesel in the presence of alcohols not only produce the desired product, but it also produces glycerol (Chattopadhyay and Sen, 2013; Rossi et al., 2013). In order to maximize the yield of usable fuel alternatives, efforts are underway to convert glycerol to products like ethanol and hydrogen (Varrone et al., 2013). To add to its significance, glycerol has been shown in the past to be anaerobically degraded by organisms such as *Desulfovibrio fructosovorans* and *D. carbinolicus* (Qatibi et al., 1998). Consequently, we reason that using another anaerobic organism, *Glk. subterraneus*, that can be grown in an MXC to directly produce current will be an added level of understanding to not only this organism, but the usefulness of this substrate. Most fortunately, it is exciting to delve into the inner-workings of such a new organism in the MXC community. As with *Geobacter, Glk. subterraneus* has the potential to become an important ARB in this community as we continue to study it to hopefully uncover its biochemical pathways for substrates of interest.

To characterize this organism, we studied its current generation and its kinetic parameters. I also measured some electrochemical parameters for each substrate. In Chapter 4, I discussed the results of our EIS experiments using *Glk. subterrnaeus*, therefore, we will

not delve into those results again. As shown in Figure 5.1, *Glk. subterraneus* couples oxidation of acetate to the production of current with anodes poised at the same previously reported value of 0.04V in a medium with pH 7.2. The cells grew within 2 days and produced significant current with a doubling time of 2.9 hrs. By the 6th day, a 1mV/s scan rate CV was done to obtain some kinetic parameters. However, when chronoamperometry resumed, the current started to decrease. Although the j_{max} is considered high (> 1A/m^2), it is not sustained at the maximum current density. Therefore, we investigated the effects of continuous flow of media on the current generation. Within minutes of establishing flow, we saw an immediate positive response in current density, which suggested that the cells were limited by an unknown nutrient present in the medium. With this setup, we were able to achieve the highest current density, 4.5 A/m^2, which the cells were able to sustain for over 10 days. When this system was restored back to batch mode, the current steadily dropped but not at a fast rate, sustaining current densities between 3 A/m^2 and 3.5 A/m^2 for about 7 days. This suggests that we have been able to have the cells overcome the nutrient barrier they experienced earlier and the true j_{max} was recorded to be 4.5 A/m^2. The acetate consumption was measured to calculate CE, which ranged from upper 50% to above 100% as has been reported in Badalamenti et al., 2013. It is suggested that these organisms find a way to produce storage polymers that can then be used when needed which is why it can be possible to have these efficiency values (Badalamenti et al., 2013).

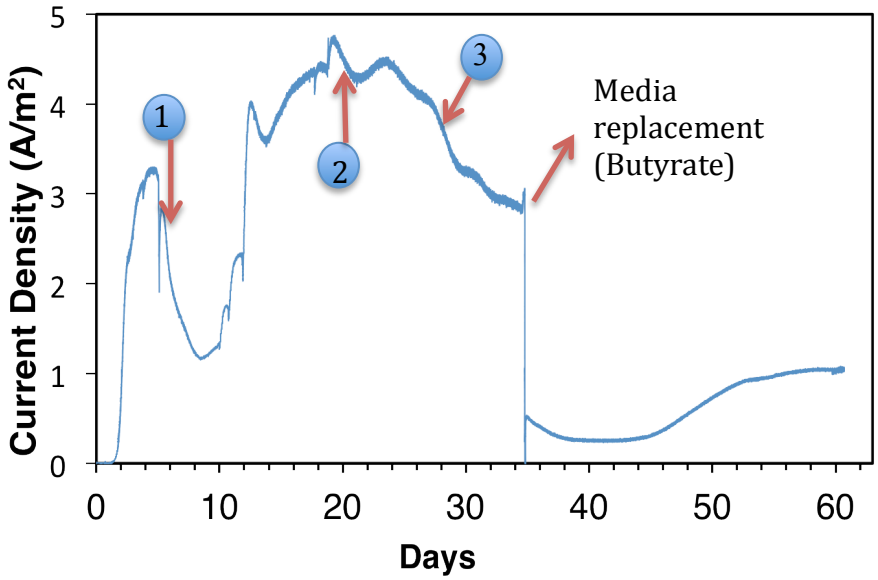

Figure 5.1. Chronoamperometry of *Glk. subterraneus* fed with 20mM acetate poised at 0.04V. At day 35, the substrate was changed to butyrate with the media replacement. The CVs are labeled as events 1, 2 and 3 respectively.

I chose to investigate the effect of a different donor on the cells by doing a media replacement with butyrate now as the donor. Since I later perform experiments with a reactor inoculated with cells that have been growing on amorphous Fe(III) oxide, the media replacement was done to have a comparison between the two methods of investigating butyrate as a donor. Not only was the media replaced, one of the anodes was also scraped clean of bacteria to confirm that current generation is from attached cells. This particular experiment is shown also in Figure 5.1. At day 35, the media was replaced with butyrate and immediately, current generated reduced to 0.5 A/m^2. However, as shown in Figure 9, the current later dropped to about half its value. This value was sustained for ~10 days before we observed an increase in current generation. There can be a few reasons for why we observed this. Firstly, there may have been residual acetate both in the biofilm and in the

media from the replacement maneuver. On the minimal acetate around, it is conceivable that the other untouched biofilm continued to produce current. When there is no more acetate around, it is understandable that the cells will have to adjust to butyrate consumption. The current eventually increased to 1.1A/m^2. This j_{max} was sustained in batch mode for approximately 10 days. At the end of this period, a CV was performed for comparison to the same biofilm fed with acetate. Butyrate consumption in this case was measured as well and its CE ranged from 40% to 62% following the same trend we saw with acetate in terms of having lower efficiencies earlier in the process of forming a new biofilm.

This approach provided us some insight as to how this halophile ARB functions with different electron donors. We already know that its list of usable donors is quite large in comparison to other bacteria in the same family and even in the same genus. However, we performed the same experiment with butyrate that we have done with acetate; we inoculated an MEC with cells previously growing on Fe (III) oxide and fed butyrate. The anodes were poised at the same potential, 0.04V, and the pH of media was kept near neutral. The cells did not produce as much current with butyrate as a donor compared to acetate. Nevertheless, we saw growth in less than 2 days with a doubling time of 6.4hrs. We have repeated these experiments two more times from smaller biofilm inoculum, but without much success. One of these attempts yielded a doubling time of 26hrs, which is much slower than any ARB we have studied. With its challenges, these experiments generated some important information such as j_{max} and other physical observations worth mentioning. No matter the doubling time, when the experiments have been successful, we have been able to obtain a maximum current density ranging from 1.4 A/m^2 to 2 A/m^2 in batch mode. All these biofilms were never as

thick (visual observation) as those formed by acetate fed cells and they tend to accumulate precipitates after 7 days of running the reactors.

The CE for butyrate experiments was ~64%, but side products like valerate, isovalerate and isobutyrate were common in our analysis both times we did these measurements. There is a possibility that one or more of these side products serve as inhibition to the production of current in these organisms. Since both isovalerate and isobutyrate are branched chain compounds and we have no metabolic information on the usage of any substrates with this organism, it is possible that these complex donors are accumulated instead. From the growth curve presented in Figure 5.2, it is evident that with butyrate as the donor, the current production drops rapidly and never recovers. I presume that another reason for this sudden drop in current is related to the concentration of butyrate available by day 4. Out of the 5mM butyrate fed, there remained 0.48mM which suggests that *Glk. subterraneus* must prefer butyrate to any other side products available in the reactor. Therefore, based on these results, it seems that, although *Glk. subterraneus* is able to consume butyrate; it is a difficult task for this particular organism.

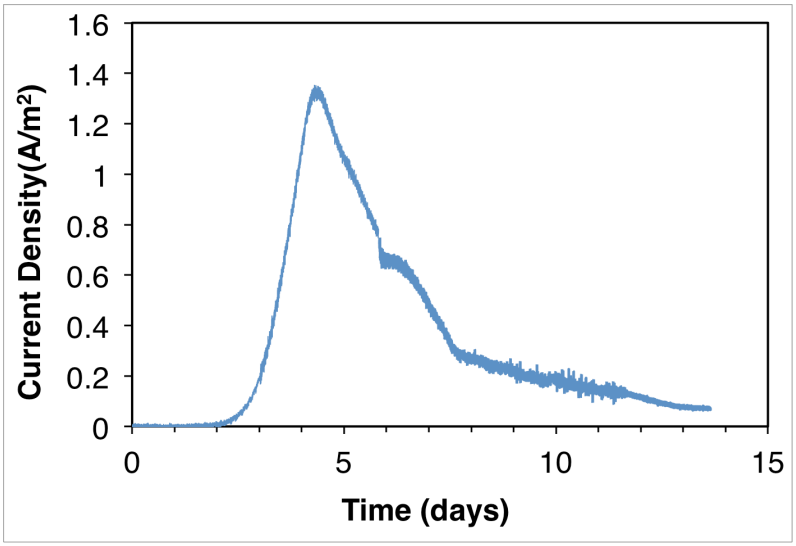

Figure 5.2: Chronoamperometry of *Glk. subterraneus* fed with 5mM butyrate poised at 0.04V in batch mode.

Glycerol, on other hand, proved to be a preferred donor for *Glk. subterraneus*. Once again everything was kept the same in the growth medium with the exception of the change, the donor (10 mM glycerol). Cells grow within 2 days of inoculation with a doubling time close to 4.8hrs. A j_{max} of about 2.3 A/m^2 was reached by day 20, and current densities between 2 and 2.5 A/m^2 were sustained over an 8 consecutive day period in batch mode. Although by day 28, current did start to drop, the cells actually resumed production of higher current densities by day 30, as shown in Figure 5.3. The noise observed in the current density measurements is probably due to an electrical connection problem between the MXC and the potentiostat. The only interruption we introduced into the system was sampling for CE measurements. Since current production continues to resume until substrate concentration starts to decrease, we can assume that there must be some accumulation of side products that may be used as reserves during certain times as the cells choose. From our CE measurements, we obtained an efficiency of 38% for glycerol consumption, but we saw fermentation of compounds such as acetate, succinate, formate

and citrate. By the end of the experiment, the glycerol concentration was very minimal. The most interesting thing I observed was an accumulation of citrate while there was slight decrease in acetate concentration (2.2 mM to 1 mM) as time elapsed. This decrease is not so significant since the amount of acetate measured was quite small. It is possible that one or more of these higher order compounds became inhibitors to the system because in all the experiments with glycerol (2 replicates), the highest current density have never been higher than 2.5 A/m^2. This may be as a result of our reactor design because in our EIS experiments with glycerol fed *Glk. subterraneus*, current densities as high as 3 A/m^2 have been recorded. Through these experiments, I have increased the repertoire of ARB capable of oxidizing more complex substrates while producing high current densities. However, given the production of by-products, there are still more questions about this organism's mechanism of glycerol utilization that deserve further investigation.

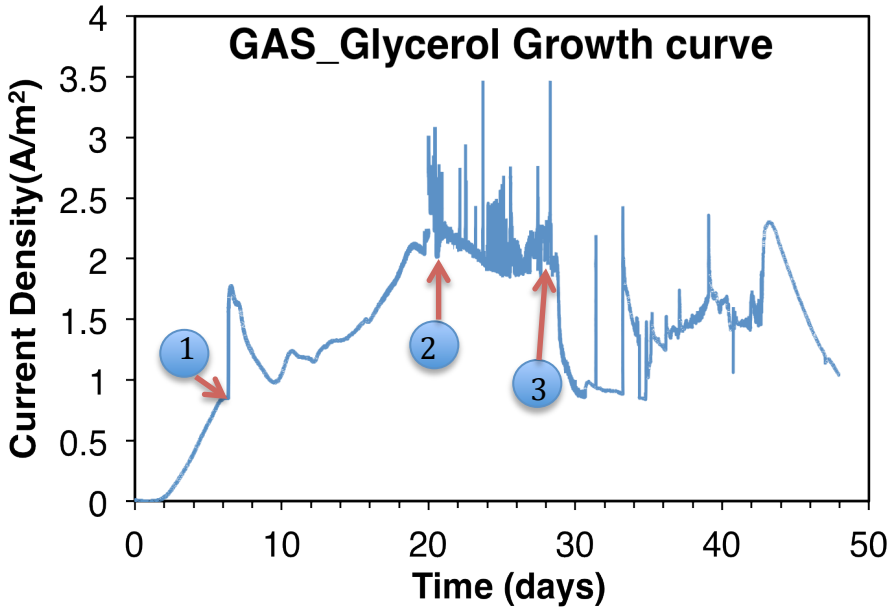

Figure 5.3: Chronoamperometry of *Glk. subterraneus* fed with 10mM glycerol poised at 0.04V. The labels represent the three CVs performed throughout the experiments.

To elucidate the kinetics involved, electrochemical measurements are paramount. The CVs I report here have been obtained with a low scan rate of 1 mV/s as we scanned over a range of potentials specified in Chapter 3. Figure 5.4 shows the variety of CVs obtained at different times throughout the duration of the experiments. A CV done earlier, day 6, is very similar to those reported for this ARB in Badalamenti et al., 2013. There are redox peaks and the forward and reverse scans are slightly separated. However, as the acetate fed biofilm ages, the separation reduces and the peaks tend to disappear. As expected, with the butyrate fed biofilms, the CVs have slight similarities to the acetate counterparts. There is, however, a major difference in the two experiments (acetate and butyrate) in that the separation in the forward and reverse scans never disappears with butyrate as the donor (data not shown). In comparison to the CVs done with butyrate biofilms, we also performed

CVs on the acetate fed biofilm that was later introduced to butyrate via a media replacement (Figure 5.5). As expected, the latter has a CV indicative of mature biofilm with no redox peaks.

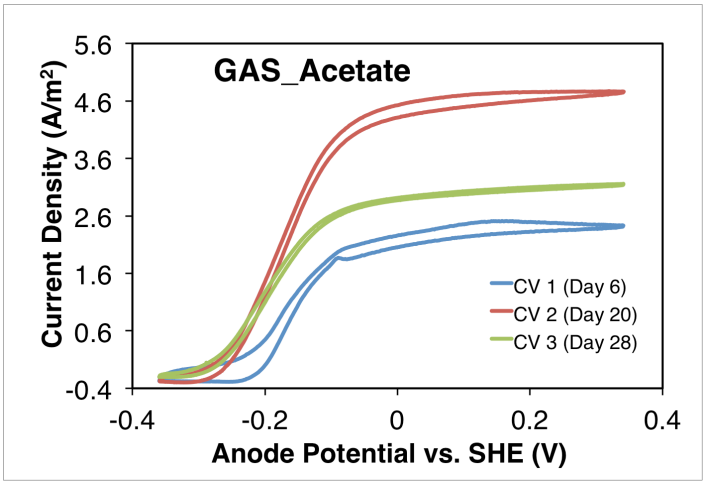

Figure 5.4. CVs of *Glk. subterraneus* grown with 20mM acetate as the donor at early; day 6, middle; day 20 and later; day 28 in the lifetime of the biofilm.

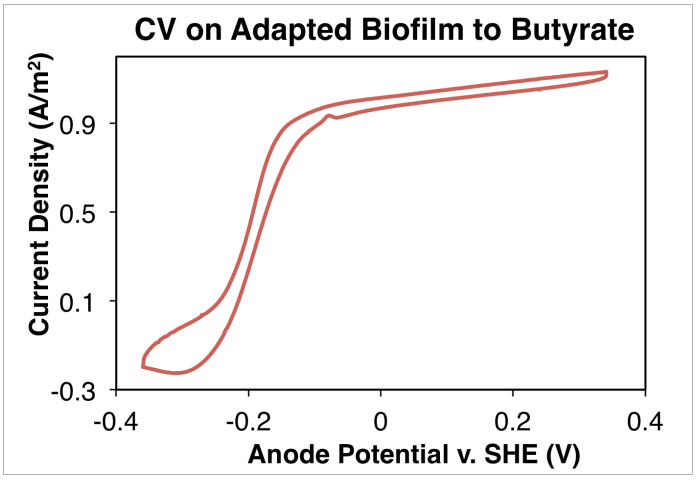

Figure 5.5. CV obtained from acetate fed biofilm after media replacement with butyrate as the donor.

The glycerol experiments also show the same progression in the shape of the CVs obtained from young to older biofilms. Redox peaks that later disappear are also present in

the earlier CVs. As with our EIS experiments, where CVs change shapes and slopes as time elapses, these CVs obtained from our glycerol fed biofilms show the same trend. Although the trend is not as obvious as with our *Geobacter* experiments (Chapter 4), it is interesting to see similar electrochemical responses in these ARB. Figure 5.6 shows the three CVs obtained from our glycerol experiments with the E_{KA} becoming slightly more negative with time.

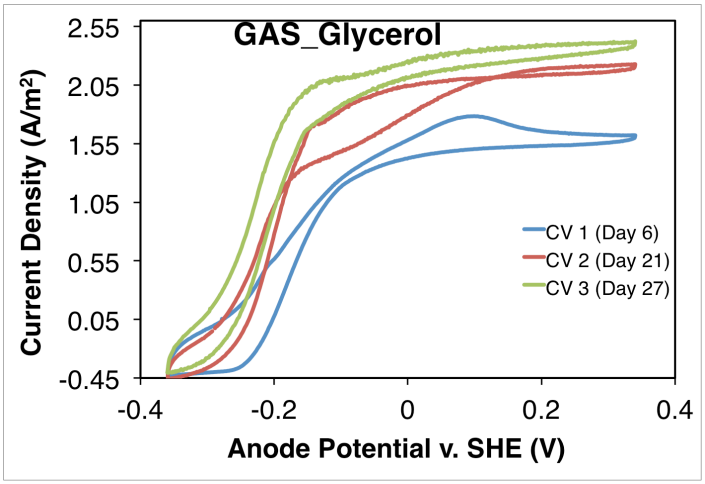

Figure 5.6. CVs of *Glk. subterraneus* grown with 10mM glycerol as the donor at early; day 6, middle; day 21 and later; day 27 in the lifetime of the biofilm.

While it is expected that the *Glk. subterraneus* CVs are not exactly alike to *Geobacter*, the model ARB, their behavior is similar, following a sigmoidal response with a comparable N-M fit. A sigmoidal curve proves that there is a biological process governing the transfer of electrons from the cells to the anode of the MECs in which they are grown. As shown in table 5.1, the Open Circuit Potential (OCP) and E_{KA} values for the donors are comparable to each other. The similar E_{KA} values suggest that *Glk. subterraneus* has conserved mechanisms for the oxidation of each donor no matter the complexity.

Table 5.1. A comparison between the electron donors showing changes in the OCP and the E_{KA}.

Donors	OCP v. SHE	E_{KA}
Acetate	-0.27 V to -0.29 V	-0.15 V to -0.18 V
Butyrate	-0.27 V	-0.17 V
Glycerol	-0.28 to -0.31 V	-0.16 V to -0.21 V

Summary and Concluding Remarks

In the journey to discovering high current density producing ARB other than *Geobacter*, we have been able to characterize a halophile, *Glk. subterraneus* as ARB that can use a variety of different organic substrates as electron donor. From CE ranging from 38% to 64%, *Glk. subterraneus* was able to utilize glycerol, acetate and butyrate as donors whose reduction can be coupled to iron reduction or anode respiration using MXCs. I have also shown the importance of CVs in characterizing a novel ARB. Using CVs, a sigmoidal response was obtained for every donor confirming electron transfer happens via a biological process. Additionally, I have shown how CVs tend to evolve over the lifetime of a study as redox peaks appear in the beginning while the biofilm is still young and these peaks disappear, as the biofilm grows older. From CVs, key parameters were also discovered to be similar for all three donors leading us to assume that *Glk. subterraneus* probably has a conserved electron-transfer mechanism independent of the complexity of the substrate. My results not only stress the importance of electrochemical methods outlined in Chapter 2, but also the need to

further understand this new ARB for applications in environments similar to that of *Glk. subterraneus*, saltwater and higher temperatures.

CHAPTER 6

RECOMMENDATIONS FOR FUTURE WORK

I have shown so far that further understanding ARB is essential for the potential applications in MXC. For further characterization of *Geobacter*, we now need to employ other methods aside from our well-known electrochemical methods discussed earlier. EIS and CVs have been able to uncover the complexity of these systems, but they have not been able to elucidate the molecular mechanisms of EET in ARB. To this end, I propose that the next step is protein film electrochemistry to investigate which cytochromes are involved in individual resistances limiting the growth of *Geobacter* to the higher current densities, as observed in the EIS experiments (Chapter 4). In the same vein, being able to understand and assign resistances to individual internal and external processes/proteins is extremely important to achieve a complete understanding of ARB's electron-transfer pathways. Since there have been discourse as to which proteins may be responsible for certain resistances, work needs to continue in this direction.

Additionally, in Chapter 4, I hinted to other measures we are taking to understand the potential gradients that develop in our systems namely low anode potential experiments. These should make clear on a macroscopic level what is taking place in our systems. We anticipate there will not be a potential gradient existing in these cells; hence, a CV obtained from these experiments should be a N-M fit of n=1 and not a sum of parallel processes. The goal here is to be able to understand how the anode potential affect the expression of the cells that ultimately colonize the anode.

EIS should continue with *Glk. subterraneus* as well. I personally think the next step with this ARB is to do EIS as a function of growth as was done with *Geobacter*. If the same

trend of potential gradient emerges, we may be able to establish a new characteristic of ARB in the *Geobacteraceae* family. Right now, the EIS we have done with *Glk. subterraneus* has been done with glycerol, as the electron donor because the cells grew better with this substrate, but it will be exciting if a fair comparison can be drawn between *Geobacter* and this halophile using acetate as the donor.

A general future direction for any ARB with regards to EIS should include a biofilm thickness study like that which was carried out in Robuschi et al., 2012. From what I discuss in Chapter 4, the charge resistances are biofilm thickness dependent and it will be an important contribution to be able to do these same experiments with the ARBs in the lab.

To continue our work on discovering and characterizing new ARBs, we have a *Geoalkalibacter* isolate, obtained from the work of Miceli et al., (2012) that needs to be microbiologically characterized. It will be a feat for an in-house isolate *Geoalkalibacter* to be able to do the same or similar exploits to the ones already known, *Glk. subterraneus* and *ferrihydriticus*. If this isolate can be characterized as a high current producing ARB, then, we would have been successful in adding to the toll of ARB than can be useful in MXC applications. In Chapter 5, I detailed our efforts to characterize *Glk. subterraneus* using different electron donors. This work can easily continue because unlike *Geobacter*, so much is still unknown about this organism. For example, when glycerol was used as the donor, it was evident from HPLC data that there are side products of glycerol metabolism and I think these could be used to understand this ARB's mechanism of metabolizing substrates.

Ultimately, since microbes are an essential part of our world, we, as researchers have the responsibility to understand them as much as we can. As stated in Chapter 1, microbes have the capacity to potentially solve a number of human problems, mainly energy. A

number of processes including food-processing industries generate wastes from which usable energy can still be harnessed. Understanding ARB and characterizing them gives us more insight into the class of microorganisms that can generate electricity from our wastes. A constant challenge facing the MXC community comes in the form of this question: how can we increase the current densities generated from our systems? The answer to this question lies in our continued investigation of ARB and what they are potentially capable of achieving in terms of converting most of the energy available in a substrate to electrical energy.

REFERENCES

Badalamenti JP, Krajmalnik-Brown R, Torres CI. 2013. Generation of High Current Densities by Pure Cultures of Anode-Respiring Geoalkalibacter spp. under Alkaline and Saline Conditions in Microbial Electrochemical Cells. *mBio* **4**:e00144–13–e00144–13.

Barton SC. 2010. Handbook of Fuel Cells. John Wiley & Sons, Ltd.

Caccavo F, Lonergan DJ, Lovley DR, Davis M, Stolz JF, McInerney MJ. 1994. Geobacter sulfurreducens sp. nov., a hydrogen- and acetate-oxidizing dissimilatory metal-reducing microorganism. *Appl. Environ. Microbiol.* **60:**3752-3759.

Chattopadhyay S, Sen R. 2013. Fuel properties, engine performance and environmental benefits of biodiesel produced by a green process. *Chem. Soc. Rev.* **105**:319–326.

Chynoweth DP, Owens JM, Legrand R. 2001. Renewable methane from anaerobic digestion of biomass. *Chem. Soc. Rev.* **22**:1–8.

Dominguez-Benetton X, Sevda S, Vanbroekhoven K, Pant D. 2012. The accurate use of impedance analysis for the study of microbial electrochemical systems. *Chem. Soc. Rev.* **41**:7228.

Ferapontova EE, Shleev S, Ruzgas T, Stoica L, Christenson A, Tkac J, Yaropolov AI, Gorton L. 2005. Perspectives in Bioanalysis Electrochemistry of Nucleic Acids and Proteins: Towards Electro- chemical Sensors for Genomics and Proteomics, ed. F. S. a. Emil Pale-ı` ek, Elsevier, vol. 1 edn, pp. 517–598.

Greene AC, Patel BKC, Yacob S. 2009. Geoalkalibacter subterraneus sp. nov., an anaerobic Fe(III)- and Mn(IV)-reducing bacterium from a petroleum reservoir, and emended descriptions of the family Desulfuromonadaceae and the genus Geoalkalibacter. *INTERNATIONAL JOURNAL OF SYSTEMATIC AND EVOLUTIONARY MICROBIOLOGY* **59**:781–785.

Jain A, O Conolly J, Wooley R, Krishnamurthy S, Marsili E. 2013. Extracellular Electron Transfer Mechanism in Shewanella loihica PV-4 Biofilms Formed at Indium Tin Oxide and Graphite Electrodes. *Int. J. Electrochem. Sci.* **8:**1778-1793.

Katuri KP, Rengaraj S, Kavanagh P, O'Flaherty V, Leech D. 2012. Charge Transport through Geobacter sulfurreducensBiofilms Grown on Graphite Rods. *Chem. Soc. Rev.* **28**:7904–7913.

Kim BH, Ikeda T, Park HS, Kim HJ, Hyun MS, Kano K, Takagi K, Tatsumi H. Electrochemical activity of an Fe(III)-reducing bacterium, Shewanella putrefaciens IR-1, in the presence of alternative electron acceptors. *Biotechnology Techniques* **13**:475–478.

Kostka JE, Luther GW III, Nealson KH. 1995. Chemical and biological reduction of Mn (III)-pyrophosphate complexes: Potential importance of dissolved Mn (III) as an environmental oxidant. *Applied and Environmental Microbiology* **59**:885–894.

Lau C, Adkins ER, Ramasamy RP, Luckarift HR, Johnson GR, Atanassov P. 2011. Design of Carbon Nanotube-Based Gas-Diffusion Cathode for O2 Reduction by Multicopper Oxidases. *Chem. Soc. Rev.* **2**:162–168.

Lin H, Szeinbaum NH, DiChristina TJ, Taillefert M. 2012. Microbial Mn(IV) reduction requires an initial one-electron reductive solubilization step. *Applied and Environmental Microbiology* **99**:179–192.

Liu Y, Bond DR. 2012. Long-Distance Electron Transfer by G. sulfurreducens Biofilms Results in Accumulation of Reduced c-Type Cytochromes. *Applied and Environmental Microbiology* **5**:1047–1053.

Logan BE. 2004. Peer Reviewed: Extracting Hydrogen and Electricity from Renewable Resources. *Environ. Sci. Technol.* **38**:160A–167A.

Logan BE. 2009. Exoelectrogenic bacteria that power microbial fuel cells. *Nat Rev Micro* **7**:375–381.

Lovley DR. 1991. Dissimilatory Fe(III) and Mn(IV) reduction. *Microbiol. Rev.* **55**:259–287.

Lovley DR. 2000. Anaerobic benzene degradation. *Biodegradation.* **11:** 107-116.

Mabbott GA. 1983. An Introduction to Cyclic Voltammetry. *J.Chem.Educ.*, **60**:697-702

Macdonald JR. 2005. Impedance Spectroscopy. Ed. Evgenij Barsoukov, J Ross Macdonald Second. Hoboken, New Jersey: John Wiley & Sons, Inc., 606 pp.

Madigan MT, Martinko JM, Dunlap PV, Clark DP. 2009. Brock Biology of Microorganisms. Twelfth ed. San Francisco, California: Pearson Education, Inc.

Malvankar NS, Lovley DR. 2012. Microbial Nanowires: A New Paradigm for Biological Electron Transfer and Bioelectronics. *Applied and Environmental Microbiology* **5**:1039–1046.

Malvankar NS, Tuominen MT, Lovley DR. 2012. Biofilm conductivity is a decisive variable for high-current-density Geobacter sulfurreducens microbial fuel cells. *Energy Environ. Sci.* **5**:5790.

Malvankar NS, Vargas M, Nevin KP, Franks AE, Ching L, Kim B-C, Inoue K, Mester T, Covalla SF, Johnson JP, Rotello VM, Tuominen MT, Lovley DR. 2011. Tunable metallic-like conductivity in microbial nanowire networks. *Nature Nanotechnology* **6:**573-579

Marsili E, Baron DB, Shikhare ID, Coursolle D, Gralnick JA, Bond DR. 2008. Shewanella secretes flavins that mediate extracellular electron transfer. *Chem. Soc. Rev.* **105**:3968–3973.

Miceli JF III, Parameswaran P, Kang D-W, Krajmalnik-Brown R, Torres CI. 2012. Enrichment and Analysis of Anode-Respiring Bacteria from Diverse Anaerobic Inocula. *Environ. Sci. Technol.* **46:**10349-10355.

Myers CR, Myers JM. 1992. Localization of cytochromes to the outer membrane of anaerobically grown Shewanella putrefaciens MR-1. *J. Bacteriol.* **174(11):**3429-3438.

Nicholson RS, Shain I. 1964. Theory of Stationary Electrode Polarography. Single Scan and Cyclic Methods Applied to Reversible, Irreversible, and Kinetic Systems. *Chem. Soc. Rev.* **36**:706–723.

O'hayre R., Cha S., Colella W., Prinz FB. 2009. Fuel Cell Fundamentals. Second ed. Hoboken, New Jersey: John Wiley & Sons, Inc.

Orazem ME, Tribollet B. 2008. ELECTROCHEMICAL IMPEDANCE SPECTROSCOPY. Hoboken, New Jersey: John Wiley & Sons, Inc., 533 pp.

Parameswaran P, Torres CI, Lee H-S, Krajmalnik-Brown R, Rittmann BE. 2009. Syntrophic interactions among anode respiring bacteria (ARB) and Non-ARB in a biofilm anode: electron balances. *Biotechnol. Bioeng.* **103**:513–523.

Parameswaran P, Torres CI, Lee H-S, Rittmann BE, Krajmalnik-Brown R. 2011. Hydrogen consumption in microbial electrochemical systems (MXCs): The role of homo-acetogenic bacteria. *Bioresource Technology* **102**:263–271.

Parameswaran P, Zhang H, Torres CSI, Rittmann BE, Krajmalnik-Brown R. 2010. Microbial community structure in a biofilm anode fed with a fermentable substrate: The significance of hydrogen scavengers. *Biotechnol. Bioeng.* **105**:69–78.

Pessanha M, Morgado L, Louro RO, Londer YY, Pokkuluri PR, Schiffer M, Salgueiro CA. 2006. Thermodynamic Characterization of Triheme Cytochrome PpcA from Geobacter sulfurreducens: Evidence for a Role Played in e -/H +Energy Transduction †,‡. *Chem. Soc. Rev.* **45**:13910–13917.

Qatibi AI, Bennisse R, Jana M, Garcia J-L. 1998. Anaerobic Degradation of Glycerol by Desulfovibrio fructosovorans and D. carbinolicus and Evidence for Glycerol-Dependent Utilization of 1,2-Propanediol. *CURRENT MICROBIOLOGY* **36:**283-290.

Qian X, Mester T, Morgado L, Arakawa T, Sharma ML, Inoue K, Joseph C, Salgueiro CA, Maroney MJ, Lovley DR. 2011. Biochemical characterization of purified OmcS, a c-type cytochrome required for insoluble Fe(III) reuction in Geobacter sulfurreducens. *Biochmica et Biophysica Acta.* **1807:**404-412.

Reguera G, McCarthy KD, Mehta T, Nicoll JS, Tuominen MT, Lovley DR. 2005. Extracellular electron transfer via microbial nanowires. *Chem. Soc. Rev.* **435**:1098–1101.

Rittmann BE. 2008. Opportunities for renewable bioenergy using microorganisms. *Biotechnol. Bioeng.* **100**:203–212.

Rittmann BE, Krajmalnik-Brown R, Halden RU. 2008. Pre-genomic, genomic and post-genomic study of microbial communities involved in bioenergy. *Nat Rev Micro* **6**:604–612.

Robuschi L, Tomba JP, Schrott GD, Bonanni PS, Desimone PM, Busalmen JP. 2012. Spectroscopic Slicing to Reveal Internal Redox Gradients in Electricity-Producing Biofilms. *Angew. Chem. Int. Ed.* **52**:925–928.

Rossi DM, de Souza EA, Flôres SH, Ayub MAZ. 2013. Conversion of residual glycerol from biodiesel synthesis into 1,3-propanediol by a new strain of Klebsiella pneumoniae. *Chem. Soc. Rev.* **55**:404–409.

Siegert M, Cichocka D, Herrmann S, Gründger F, Feisthauer S, Richnow H-H, Springael D, Krüger M. 2010. Accelerated methanogenesis from aliphatic and aromatic hydrocarbons under iron- and sulfate-reducing conditions. *Environ. Sci. Technol.* **315**:6–16.

Strycharz-Glaven SM, Tender LM. 2012. Study of the Mechanism of Catalytic Activity of G. Sulfurreducens Biofilm Anodes during Biofilm Growth. *ChemSusChem* **5**:1106–1118.

Torres CSI, Marcus AK, Lee H-S, Parameswaran P, Krajmalnik-Brown R, Rittmann BE. 2010. A kinetic perspective on extracellular electron transfer by anode-respiring bacteria. *FEMS Microbiology Reviews* **34**:3–17.

Torres CI, Marcus AK, Rittmann BE. 2007. Kinetics of consumption of fermentation products by anode-respiring bacteria. *Appl Microbiol Biotechnol* **77**:689–697.

Torres CI, Marcus AK, Rittmann BE. 2008. Proton Transport Inside the Biofilm Limits Electrical Current Generation by Anode-Respiring Bacteria. *Biotechnology and Bioengineering* **100:**872-881.

Varrone C, Liberatore R, Crescenzi T, Izzo G, Wang A. 2013. The valorization of glycerol: Economic assessment of an innovative process for the bioconversion of crude glycerol into ethanol and hydrogen. *Chem. Soc. Rev.* **105**:349–357.

Weber KA, Achenbach LA, Coates JD. 2006. Microorganisms pumping iron: anaerobic microbial iron oxidation and reduction. *Nat Rev Micro* **4**:752–764.

Welch VA, Fallon KJ, Gelbke HP. 2005. "Ethylbenzene" Ullmann's Encyclopedia of Industrial Chemistry, Wiley-VCH, Weinheim. doi:10.1002/14356007.a10_035.pub2

Yi H, Nevin KP, Kim B-C, Franks AE, Klimes A, Tender LM, Lovley DR. 2009. Selection of a variant of Geobacter sulfurreducens with enhanced capacity for current production in microbial fuel cells. *Chem. Soc. Rev.* **24**:3498–3503.

Zavarzina DG, Kolganova TV, Boulygina ES, Kostrikina NA, Tourova TP, Zavarzin GA. 2006. Geoalkalibacter ferrihydriticus gen. nov. sp. nov., the first alkaliphilic representative of the family Geobacteraceae, isolated from a soda lake. *Microbiology* **75**:673–682.

APPENDIX A

CHARACTERISTIC DIFFERENCES IN *GLK. FERRIHYDRITICUS* AND *GLK. SUBTERRANEUS*

Characteristic	*Geoalkalibacter subterraneus*	*Geoalkalibacter ferrihydriticus*
DSMZ designation	23483	17813
Temperature optimum (°C)	40	35
Temperature range (°C)	30–50	18–39
pH optimum	7.0	8.5
ph range	6–9	7.8–10
Motility	+	+
DNA G+C content (mol%)	52.5	55.3
Salinity range (% w/v NaCl)	0.1−10	0−5
Salinity optimum (% NaCl)	2	0.1
Electron acceptors		
AQDS	ND	+
Fe(III) oxide, amorphous	+	+
Fe(III)-EDTA	ND	+
Fe(III)-citrate	+	−
Fumarate	−	−
Mn(IV)	+	+
Nitrate	+	−
S^0	+	+
Sulfate	−	−
Electron donors		
Acetate	+	+
Butyrate	+	−
Ethanol	+	+
Formate	+	−
Glycerol	+	−
Hydrogen	+	−
Malate	−	ND
Malonate	+	−
Methanol	+	−
Palmitate	+	ND
Peptone	+	−
Propionate	+	+
Pyruvate	+	+
Stearate	+	ND
Succinate	+	−
Yeast extract	+	−

APPENDIX B

ELECTROCHEMICAL IMPEDANCE SPECTROSCOPY RESULTS OF REPLICATE EXPERIMENTS

Here, I have outlined the results of the EIS replicate experiments, specifically reactors 1 and 2, since results for reactor 3 have been outlined in chapter 4. The central theme here is that the results were similar all times the experiments were carried out.

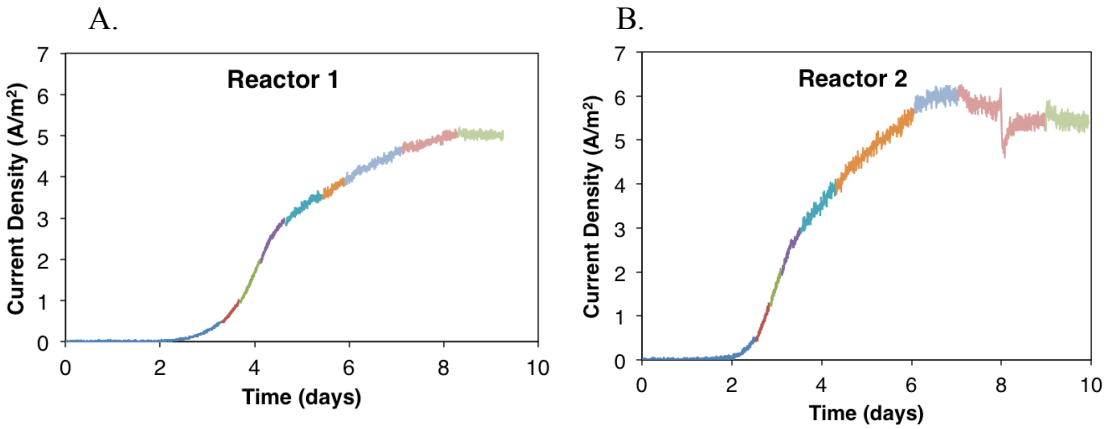

Figure 1. The growth curves obtained from experiment #1(A.) and #2 (B.) consecutively. EIS measurements were obtained at the end of each color segment

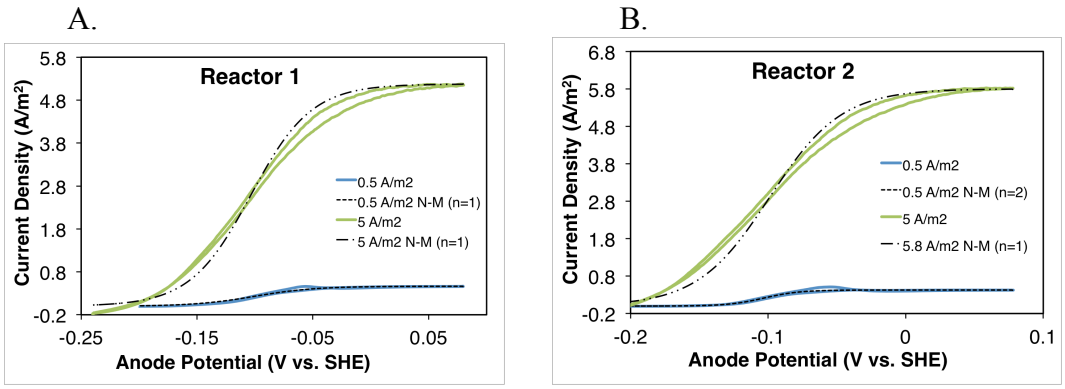

Figure 2. CVs obtained at different growth stages showing the evolution of the shapes of both CVs as a function of growth.

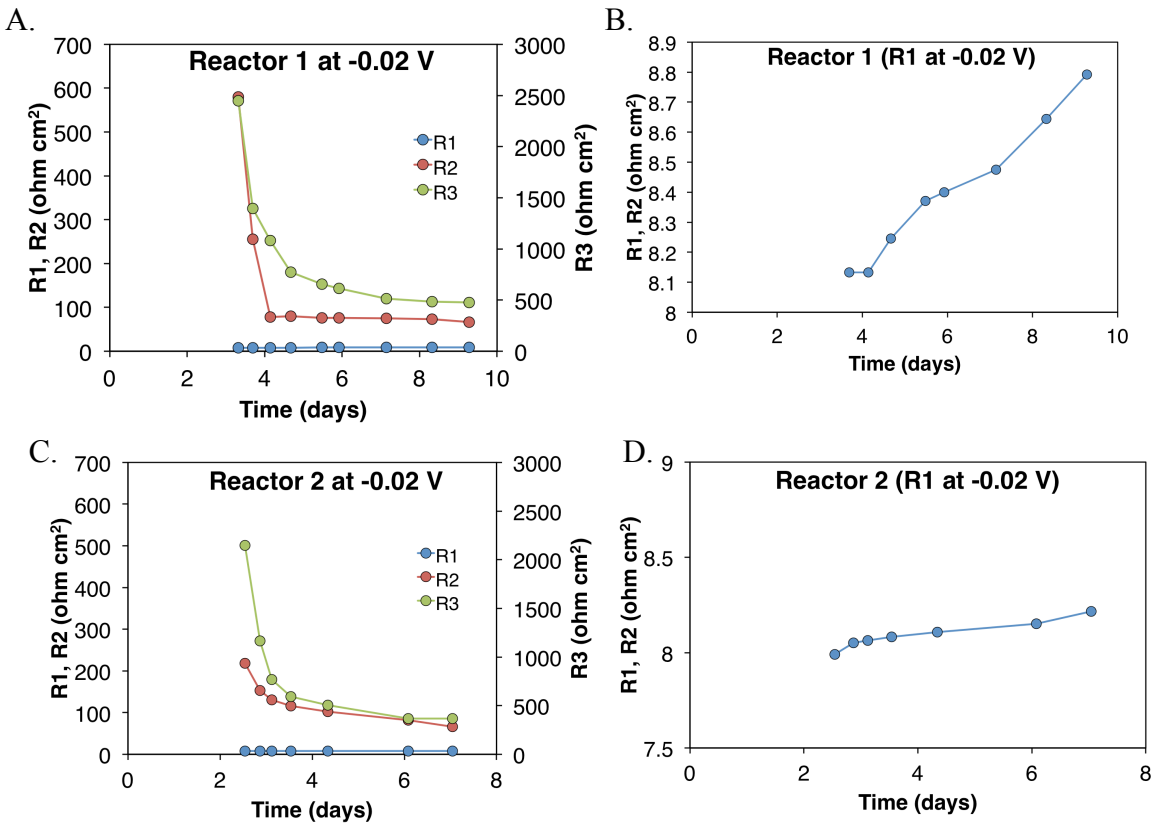

Figure 3. Ohmic resistances as represented in experiments #1 and #2 are shown in comparison to other resistances in (A.) and (C.) while (B.) and (D.) show the slight increase in ohmic resistances.

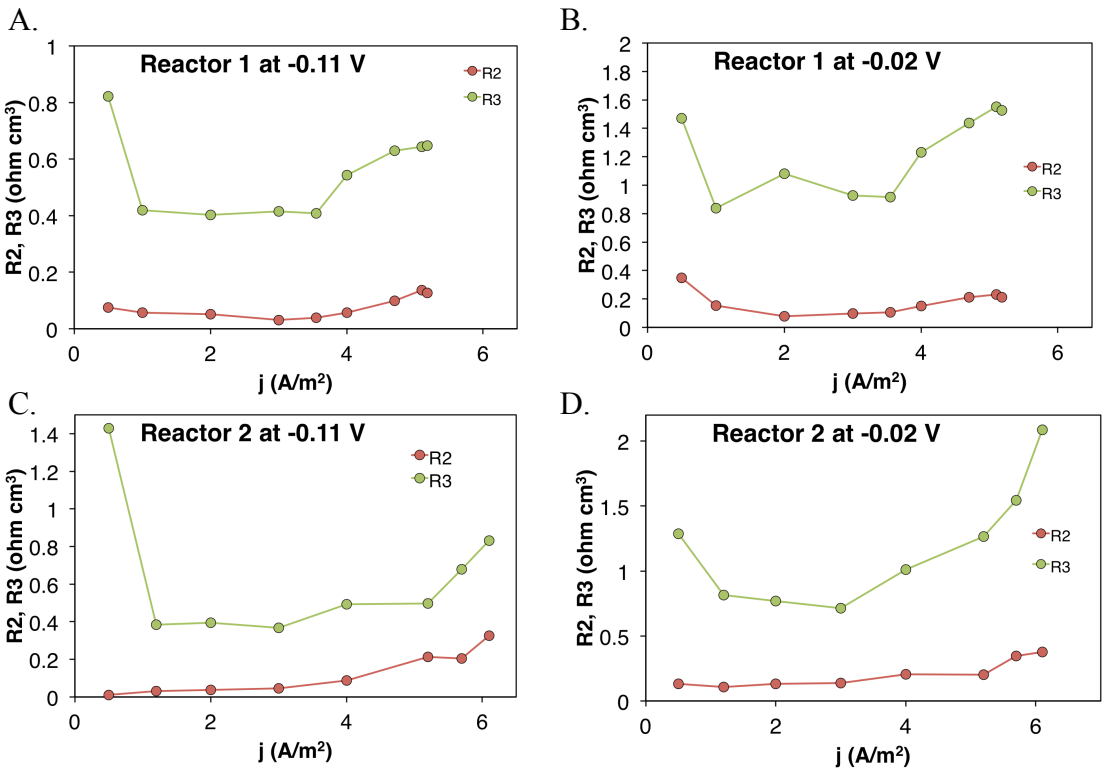

Figure 4. The two charge transfer resistances, R2 and R3, obtained at both potentials, -0.02V and -0.11V are shown here with R3 always higher than R2.

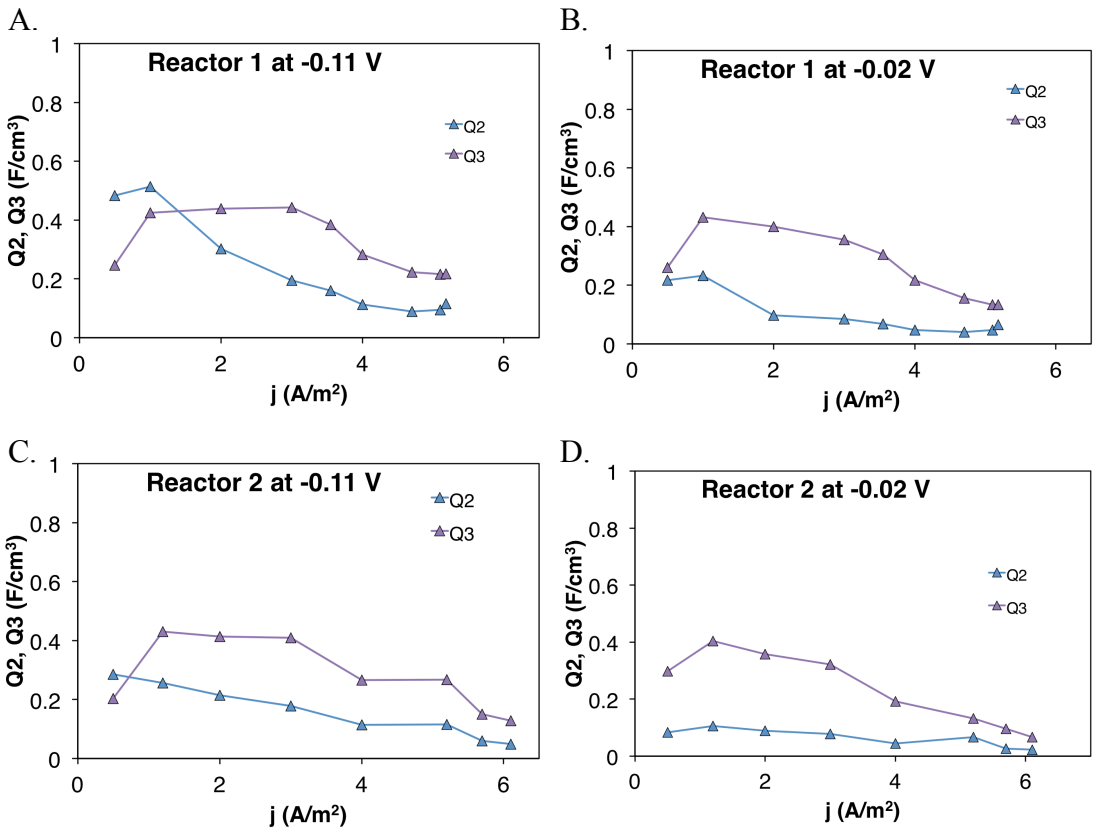

Figure 5. Shown here are the capacitance measurements at both potentials at which EIS measurements were obtained.